气象科技进展 Advances in Met S&T

DOI：10.3969/j.issn.2095–1973.2015.03.002

天气和气候模式中的质量通量型大气对流参数化

张广俊[1, 2]

（1 清华大学地球系统科学中心，北京 100084；2 斯克里普斯海洋研究所，美国）

0 引言

自数值天气预报和气候模拟出现伊始，数值模式对大气对流的描述或参数化就一直是一项具有挑战性的任务。单个对流单体具有很小的空间和时间尺度，空间上大约小于一到数十千米，时间上从几分钟到数小时。有组织的对流系统，比如飑线和中尺度对流复合体，其规模可达数百千米，时间上可持续一天甚至更长。对流是大气环流的一个重要能量来源，尤其是在热带。从社会经济角度来看，对流常常与暴洪、龙卷及飓风/台风等给社会带来极大经济损失的高影响极端天气联系在一起。因此，准确预报对流或强风暴发生的时间和地点，对于数值天气预报而言是重中之重。鉴于对流具有很小的空间尺度，其无法通过全球气候模式（General Circulation Models, GCM）和数值天气预报（Numerical Weather Prediction, NWP）模式得到解决，而只能通过参数化方法。

大气对流中质量、热量和水汽垂直输送的参数化一直是极为困难的问题，因为对流与云、大气水汽和辐射具有强烈的相互作用，其过程在空间和时间尺度上跨越数个数量级。20世纪后半叶以来，科学家们已开发出多个参数化方案，从简单的对流调整方案[1-2]到水汽辐合方案[3-5]以及基于对流不稳定能量的质量通量方案[6-9]。随着我们对对流及其与大尺度环流和云相互作用认识的不断深入，对流参数化涵盖了越来越多的物理过程，包括动量对流输送[10-13]和对流云微物理过程[14-17]。从气候变化研究的角度分析，云和气溶胶是影响气候预估不确实性的两个最重要的因素[18]，而两者均与对流密切相关。在热带，云经常通过对流产生，上升气流中云水和云冰的卷出形成砧状云，其对地球辐射的收支具有重大影响。气溶胶不仅对大气辐射有直接作用，同时也可成为云凝结核和冰核。对流可垂直传输气溶胶，降雨的清除和冲刷也能影响大气中气溶胶的沉降。近年的观测结果也表明气溶胶对对流有重要的影响[19-20]。

本文将对对流参数化的发展予以全面回顾，重点关注降水性深对流。第一部分简要介绍早期对流参数化的发展，第二部分对数个质量通量型对流参数化方案进行评述；第三部分对对流动量输送参数化予以回顾；而第四部分对近期相关进展和仍待解决的问题进行探讨，并且给出总结性评述。

收稿日期：2013 年 6 月 13 日；修回日期：2014 年 1 月 15 日

第一作者：张广俊（1960—），Email: zhangguangjun1960@gmail.com

资助信息：美国能源部科学办公室项目[（BER）DE-SC0000805]；美国国家科学基金会项目（AGS-1015964，EaSM-1048995）；美国国家海洋和大气管理局项目（NA08OAR4320894）

1 早期对流参数化

在早期的全球气候模拟中，人们对对流加热在大尺度环流中的作用已经有所认识。Manabe等[1]是最早利用对流调整并将其纳入地球物理流体动力实验室（Geophysical Fluid Dynamics Laboratory，GFDL）模式的研究人员之一，该理念和方法简单实用：在某一大气层中如果气温垂直递减率超过了中性层结，则立刻进行调整以去除这一不稳定性。对不饱和大气，如果

$$-\frac{\partial T}{\partial p} > \gamma_d$$

则

$$\begin{aligned} &\delta q = 0 \\ &\frac{\partial}{\partial p}\theta(T+\delta T, p) = 0 \\ &\int_{p_B}^{p_T} \delta T \mathrm{d}p = 0 \end{aligned} \qquad (1)$$

式中，γ_d为干绝热递减率，δq为水汽混合比调整量，δT为温度调整量，θ为位温，p_T和p_B分别为干调整时大气顶层和大气底层温度。通过式（1）可得到每一模式层的温度调整量。同理，对于饱和大气，大气层的湿度调整需满足下列方程组

如果

$$-\frac{\partial T}{\partial p} > \gamma_m$$

则

$$\begin{aligned} &\frac{\partial}{\partial p}\theta_e(T+\delta T, q+\delta q, p) = 0 \\ &q+\delta q = q_s(T+\delta T, p) \\ &\int_{p_B}^{p_T} c_p \delta T + L\delta q \mathrm{d}p = 0 \end{aligned} \qquad (2)$$

式中，θ_e为相当位温，q_s为饱和水汽混合比，c_p和L分别为恒压比热和凝结潜热。通过求解式（2）可得到δT和δq。尽管很简单，但这一调整方法解释了在对流层中次网格尺度对流、大气加热和对流层水汽耗散最根本的影响效应。

同一时期，为了将对流影响纳入飓风模拟中，Kuo[3-4] 开发了一个对流参数化方案，将深对流单体认定为将湿热表层大气输送到对流层的“热塔” [21]。Kuo[3-4]引入了云模式，在此模式中对流的潜热释放是通过云内的垂直运动实现而不是如Manabe等[1]通过局部调整实现。对流通过暖云气块与其周围环境的混合总体影响着网格尺度温度。

Kuo[3-4]方案假设：（1）对流发生在大气条件不稳定及低层水平水汽辐合的地区；（2）对流云起源于边界层，云中温、湿廓线可通过典型边界层大气假湿绝热线描述；（3）云从边界层空气的抬升凝结高度起至气块的中性浮力高度。这一方案的关键参数是降水量，其可估算大气气柱的净凝结加热。在以上假设下，Kuo[3-4]方案以气柱的大尺度水汽方程垂直积分为起点：

$$\int_0^{p_s}\frac{\partial \overline{q}}{\partial t}\mathrm{d}p=-Pg-\int_0^{p_s}\nabla\cdot(\overline{\boldsymbol{v}}\,\overline{q})\mathrm{d}p+gF_{LH}=g(M_t-P) \quad (3)$$

其中

$$M_t=-\frac{1}{g}\int_0^{p_s}\nabla\cdot(\overline{\boldsymbol{v}}\,\overline{q})\mathrm{d}p+F_{LH} \quad (4)$$

包括水平辐合和表面蒸发（F_{LH}）的空气柱总水汽供应。P为表面降水，等于净凝结率的气柱垂直积分

$$P=\frac{1}{g}\int_0^{p_s}(c-e)\mathrm{d}p \quad (5)$$

式（4）中$\overline{\boldsymbol{v}}$，$\overline{q}$分别表示 v, q的大尺度平均。Kuo[3-4]假定小部分的水汽供应（bM_t）用以加湿大气，其余的成为降水，即

$$P=(1-b)M_t \quad (6)$$

式中，b为可调参数。因此，通过大尺度场计算得到总水汽供应（M_t）后就可计算出表面降水P及潜热加热的气柱垂直积分。由于式（3）~（6）以气柱的垂直积分形式给出，为了确定对流运动对各模式层温度场的影响，必须给定加热的垂直分布。Kuo[3-4]进一步假设凝结加热与沿假湿绝热线运动的云中气块和环境空气的温度差成比例。因此

$$L(c-e)=\frac{gLP}{p_b-p_t}\frac{T_c-\overline{T}}{<T_c-\overline{T}>} \quad (7)$$

式中，角括号表示云层的垂直平均，P_b和P_t分别为云底和云顶的压力，云层外潜热加热为零。

20世纪60年代末和70年代初，其他研究团队也活跃于对流参数化研究领域[22-23]。不同于通过云中空气与环境空气的混合来加热大尺度大气的概念，他们引入了补偿性下沉的概念。在这一框架下，对流上升气流将气块从对流层表层输送至上层，通过气块的不断输送，对流环境中发生补偿性下沉，进而对周围大气产生干绝热加热。Kuo[4]指出尽管解释不同，但是他的方法与基于质量通量思路的大气对流加热的机制是相同的。

Kuo方案最主要的缺点是对水汽场没有预测能力，因为假设了水汽幅合的一部分用来加湿大气。因为这个假设缺陷，Kuo方案在数值模式中没有得到广泛应用；虽然在个别模式中应用很成功[24]。

2 质量通量参数化

迄今有关对流参数化最复杂、最经典的成果是Arakawa等[6]于1974年出版的论著，它为目前在数值预报和全球气候模式中应用的绝大部分质量通量对流参数化方案奠定了基础。因此在这一节中我们将对这类方案加以论述。通常的对流参数化方案假设对流发生在空间尺度数千米以下，因此对模式分辨率而言是次网格尺度。大尺度温度和湿度场的控制方程[25]为

$$\frac{\partial \overline{s}}{\partial t}+\nabla\cdot(\overline{\boldsymbol{v}}\,\overline{s})+\frac{\partial(\overline{\rho}\,\overline{w}\,\overline{s})}{\overline{\rho}\partial z}=\overline{Q}_R+L(c-e)-\nabla\cdot(\overline{\boldsymbol{v}'s'})-\frac{\partial\overline{\rho}\,\overline{w's'}}{\overline{\rho}\partial z} \quad (8)$$

$$\frac{\partial \overline{q}}{\partial t}+\nabla\cdot(\overline{\boldsymbol{v}}\,\overline{q})+\frac{\partial(\overline{\rho}\,\overline{w}\,\overline{q})}{\overline{\rho}\partial z}=-(c-e)-\nabla\cdot(\overline{\boldsymbol{v}'q'})-\frac{\partial\overline{\rho}\,\overline{w'q'}}{\overline{\rho}\partial z} \quad (9)$$

式中，$s=C_pT+gz$ 是干静力能，q为比湿，v是水平风矢量，w是垂直速度，L为汽化潜热。上划线表示大尺度区域或模式网格平均，撇号为相对与平均而言的偏差。右端的扰动乘积项表示次网络输送（如对流）对大尺度或网格平均场的效应。Q_R为辐射加热率，$c-e$代表GCM网格内的净凝结。在式（8）和（9）中我们略去了凝华/升华和冻结/融化过程中的加热。一般来说，因扰动通量的水平辐散比垂直辐散要小得多而予以忽略。因此，对流运动对大尺度温度和湿度场的效应可表示为

$$\left(\frac{\partial \bar{T}}{\partial t}\right)_c = \left(L(c-e) - \frac{\partial \bar{\rho}\overline{w's'}}{\bar{\rho}\partial z}\right) \Big/ C_p \qquad (10)$$

$$\left(\frac{\partial \bar{q}}{\partial t}\right)_c = -(c-e) - \frac{\partial \bar{\rho}\overline{w'q'}}{\bar{\rho}\partial z} \qquad (11)$$

为将这些效应用大尺度变量参数化，任意变量x可表示为$x=\bar{x}+x'$，其中$\bar{x}=\frac{1}{A}\int x\mathrm{d}A$是在区域A的$x$平均值，$x'=x-\bar{x}$。因此，$\overline{x'}=0$。假设在此区域中有数块积云占据着区域$A_c$，无对流活动的区域为$A$-$A_c$（图1），对流活动区域内$x$的平均值为$x_c$，而无对流活动区域中$x$的平均值为$x_e$，则

$$\begin{aligned}\bar{x} &= (A_c x_c + (1-A_c)x_e)/A = \sigma x_c + (1-\sigma)x_e \\ x_c' &= x_c - \bar{x} = (1-\sigma)(x_c - x_e) \\ x_e' &= x_e - \bar{x} = -\sigma(x_c - x_e) = -\frac{\sigma}{1-\sigma}x_c'\end{aligned} \qquad (12)$$

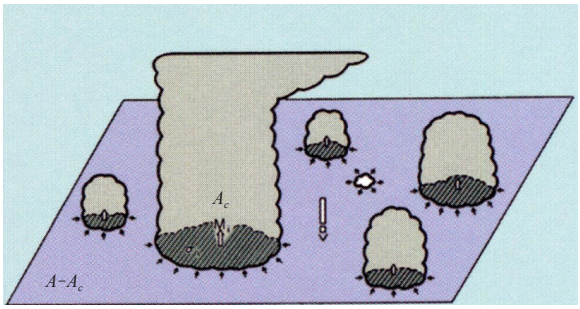

图1 典型的气候模式网格示意图
（网格中有数个积云，占总面积A_c，无对流区占总面积1–A_c）
Fig.1 Schematic showing a typical model grid box, in which there are a number of convective clouds occupying a total area of A_c, the convection–free area of the grid box is 1–A_c

式中，$\sigma=A_c/A$为对流云所占相对区域。如果我们进一步假设在云区及环境中x'和y'不相关，利用式（12），变量x和y的乘积的涡动相关可表示为

$$\begin{aligned}\overline{x'y'} &= \sigma(x'y')_c + (1-\sigma)(x'y')_e = \sigma x_c' y_c' + (1-\sigma)x_e' y_e' \\ &= \sigma x_e' y_e' + (1-\sigma)(-\frac{\sigma}{1-\sigma}x_c')(-\frac{\sigma}{1-\sigma}y_c') = \frac{\sigma}{1-\sigma}x_e' y_e' \\ &= \frac{\sigma}{1-\sigma}(x_c-\bar{x})(y_c-\bar{y})\end{aligned} \qquad (13)$$

对于干静力能（s）的垂直输送，令

$$y=s, x=w$$

则

$$\bar{\rho}\overline{w's'} = \frac{\sigma}{1-\sigma}\bar{\rho}(w_c-\bar{w})(s_c-\bar{s}) \qquad (14)$$

对于如GCM的数值模式，水平分辨率大约为100km或以上，对流活动所占区域通常很小，$\sigma \ll 1$，$\bar{w} \ll w_c$，因此式（14）可简化为

$$\bar{\rho}\overline{w's'} \approx \sigma\bar{\rho}w_c(s_c-\bar{s}) = M_c(s_c-\bar{s}) \qquad (15a)$$

式中，$M_c=\sigma\bar{\rho}w_c$为云的质量通量。如果将上升气流和下沉气流均予以考虑，则上式应表示为

$$\bar{\rho}\overline{w's'} = M_u(s_u-\bar{s}) + M_d(s_d-\bar{s}) \qquad (15b)$$

式中，下标u和d分别表示上升气流和下沉气流。对于数值预报模式或高分辨率全球气候模式，模式格距可小至10km，则不能再忽略对流所占区域。在此情况下，式（14）中的所有项均需保留，而近似式（15a）和（15b）不能成立，后面将对此做进一步的论述。

有了式（15b），考虑了对流效应的大尺度场温度和湿度收支方程为

$$\frac{\partial \bar{s}}{\partial t} + \nabla\cdot(\bar{v}\,\bar{s}) + \frac{\partial(\bar{\rho}\,\overline{ws})}{\bar{\rho}\partial z} = \bar{Q}_R + L(c-e) - \frac{\partial}{\bar{\rho}\partial z}[M_u(s_u-\bar{s}) + M_d(s_d-\bar{s})] \qquad (16)$$

$$\frac{\partial \bar{q}}{\partial t} + \nabla\cdot(\bar{v}\,\bar{q}) + \frac{\partial(\bar{\rho}\,\overline{wq})}{\bar{\rho}\partial z} = -(c-e) - \frac{\partial}{\bar{\rho}\partial z}[M_u(q_u-\bar{q}) + M_d(q_d-\bar{q})] \qquad (17)$$

式（16）和（17）是所有质量通量对流参数化方案的起点。很显然，要参数化大尺度温度和湿度场的对流效应，就必须了解云的质量通量、云内温湿度以及对流上升气流和下沉气流内的凝结和蒸发，这可通过引入简单的定常态上升和下沉模式，以及闭合假设来实现。

2.1 云模式

2.1.1 定常态模式

对流云中的上升和下沉气流通常被认为由一缕缕气团组成。为参数化起见，假设积云处于定常态。这种情况下，云内物理属性可由如下方程描述

$$\frac{\partial F}{\rho \partial z} = \text{source} - \text{sink}$$

式中，F为一模式层上下界面的物理量通量，source和sink为模式层内的源与汇。它既可产生于云内也可由侧边界输送进来。对于上升气流内的质量通量、热量、湿度和云凝结，方程为[9]

$$\frac{\partial M_u}{\rho \partial z} = E_u - D_u \tag{18}$$

$$\frac{\partial M_u s_u}{\rho \partial z} = E_u \overline{s} - D_u \hat{s}_u + L(c-e) \tag{19}$$

$$\frac{\partial M_u q_u}{\rho \partial z} = E_u \overline{q} - D_u \hat{q}_u - (c-e) \tag{20}$$

$$\frac{\partial M_u l}{\rho \partial z} = -D_u l + (c-e) - R_r / \rho \tag{21}$$

式中，E_u和D_u是气块夹卷和卷出，s_u和q_u是上升气流中的干静力能和比湿。假设上升气流中的空气为饱和

$$q_u = q_s(s_u) \tag{22}$$

式中，$\hat{s}_u$和$\hat{q}_u$是卷出到环境空气的干静力能和水汽。在卷出层，通常假设其空气与环境空气的温度相同且为饱和，

$$\hat{s}_u = \overline{s} \tag{23}$$

$$\hat{q}_u = q_s(\overline{s}) \tag{24}$$

式（21）中，假设卷出到环境空气中的云液态水与同一层上升气流平均液态水相同，R_r是云液态水变为雨水的转换率，可作为第一级近似设为与l成正比[5,6,9,26]

$$R_r = c_0 M_u l \tag{25}$$

式中，$c_0 = 2\times10^{-3}\text{m}^{-1}$。注意此式没有考虑冻结，因此在（21）式中$l$代表总凝结量。在NCAR CAM5中采用的Zhang-Mcfarlane方案里，上升气流的总凝结量进一步基于温度区分为云水和冰，在大尺度温度方程中考虑了卷出冰冻结产生的潜热加热。

在这个简单定常态一维模式中，对流上升气流中云的微物理过程仅在式（25）中通过一个可调参数非常粗略地参数化。近期的若干研究[19-20]表明气溶胶对对流云的发展有重要的影响，要反映气溶胶对对流的影响就需要在对流参数化中考虑云的微物理过程。另外，云冰和水的对流卷出是大尺度云或砧状云的重要来源，大尺度云或砧状云对地球的辐射收支具有根本性影响。鉴于气溶胶-对流-云-辐射相互作用的重要性，对对流微物理过程的过度简化处理是明显不合适的。近年研究者开发了一些较复杂的对流微物理过程方案[14-17]，感兴趣的读者可参阅相关论著。

我们需要知道式（18）～（21）中上升气流的质量通量，这由给定对流卷入、卷出来决定。Tiedtke[5]将夹卷划分为有组织的入流和湍流夹卷，气块卷出分为有组织的出流和湍流卷出

$$E_u = E_u^1 + E_u^2,\ D_u = D_u^1 + D_u^2 \tag{26}$$

式中，$E_u^1 = \varepsilon_u M_u$，$D_u^1 = \delta_u M_u$分别是湍流卷入和湍流卷出。分数夹卷率（fractional entrainment rate）ε_u和δ_u与云的种类有关。对于在对流抑制条件下的浅对流，$\varepsilon_u = \delta_u = 3\times10^{-4}\text{m}^{-1}$。对存在大尺度辐合的深对流和中层对流，$\varepsilon_u = \delta_u = 1\times10^{-4}\text{m}^{-1}$。对深对流和浅对流取不同值旨在模仿浅对流云小，因而其边界上会有更多夹卷；而深对流云面积大，受夹卷影响小。对有组织的卷入，Tiedtke[5]假设其与大尺度水汽辐合成正比

$$E_u^2 = -\frac{\overline{\rho}}{\overline{q}}\left(\overline{\boldsymbol{v}} \cdot \nabla \overline{q} + \overline{w}\frac{\partial \overline{q}}{\partial z}\right) \tag{27}$$

对浅对流，不考虑有组织的夹卷，因为浅对流通常发生在大尺度下沉气流区。深对流有组织的卷出发生在对流云最高层，所有对流质量通量都在那里卷出。浅对流系统性卷出发生在云顶以下的最高两层。70％质量通量在零浮力层卷出，30％在其上一层卷出，代表过度穿越（overshooting）。卷入、卷出给定后，可以对式（18）～（25）积分，得到对流上升气流中云的属性。

多气流模式（ensemble-plume-based model）通常只考虑湍流卷入和湍流卷出[6,9]。分数夹卷率通过更为复杂的方法被确定。对分数夹卷率为λ的云型质量通量随高度的变化表示为

$$\frac{\partial m_u(\lambda, z)}{\partial z} = \lambda m_u(\lambda, z) \tag{28}$$

将所有对在高度z的质量通量有贡献的λ积分，得到

$$M_u(z) = \int_0^{\lambda_D(z)} m_u(\lambda, z)\mathrm{d}\lambda \tag{29}$$

式中，$\lambda_D(z)$是在高度z卷出的上升气流所对应的分数夹卷率。这里隐含地假设了$\lambda_D(z)$随高度单调递减。因此，夹卷率$\lambda > \lambda_D(z)$的云对z高度的质量通量没有贡献。λ_D取决于高度z处卷出云的温度与环境温度相同这一必要条件，而这可由式（30）来保证

$$h_b - h^*(z) = \lambda_D(z)\int_{z_b}^{z}\left[h_u(\lambda, z') - h_b\right]\mathrm{d}z' \tag{30}$$

式中，h_u是分夹卷率为λ的上升气流的湿静力能，h^*是饱和湿静力能。对于某一云型，有组织的卷出发生在云顶。因为我们考虑了整个云谱，有组织的卷出可以发生在所有层，这与Tiedtke[5]方案不同

$$D_u(z) = -m_u[\lambda_D(z), z]\frac{\mathrm{d}\lambda_D(z)}{\rho \mathrm{d}z} \tag{31}$$

由此，上升气流卷出质量E_u可由式（18）得出。一旦知道云的质量通量的垂直分布，则其他物理量即可通过式（19）～（25）确定。注意，对一个给定的

云型分数卷入率，假设其随高度不变，但是近年来的研究发现对流夹卷率随高度显著变化[27-29]。由于卷入率在确定对流从日循环到季节内振荡（Maddan-Julian Oscillation，MJO）中具有重要意义，相关研究近来成为研究热点。

下沉气流模式与倒置的上升气流相近。在初始处的下沉气流质量通量通常与云底上升气流质量通量成正比[30]。另外，下沉气流的卷出通常在云底以上不考虑，而其卷入率或者是给定的或者与上升气流卷入率相关。详尽内容可参见[9]。

2.1.2 间隙性混合模式

夹卷气流型云模式假设云下空气进入云后在上升过程中与卷入的环境空气彻底混合。相反，Raymond等[31]引进了随机混合概念，其中假设一个单个云下气块在其上升到零浮力层并卷出前只有一次混合过程。基于这种间隙性混合概念，Emanuel[7]提出了随机混合云模式来表达对流上升气流。在这种模式中，每一个量级为O（1km）的云由许多量级为O（100m）的上升气流组成。一团上升气流从云底到某一高度，在其上升过程中具有相同概率与所经高度的环境空气混合。混合后的空气或升或降，取决于其浮力。在这种通过浮力筛选的模式中，积云质量通量由浮力的垂直梯度决定。图2给出混合型云的流程图。详细的数学表达比较复杂，这里不再详述。扩展阅读请参考Emanuel[7]和Emanuel等[32]的研究成果。

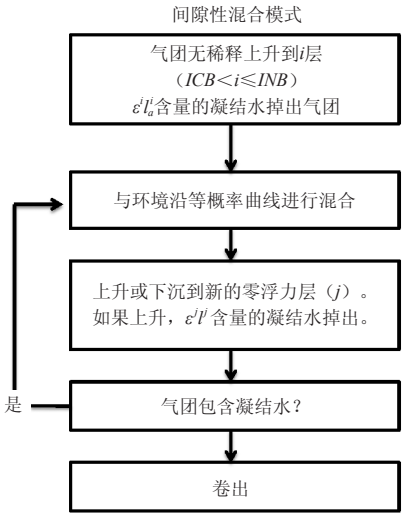

图2 间隙性混合模式流程图[7]

Fig. 2 Flow chart for episodic mixing model[7]

2.2 闭合条件

只有在得到云底质量通量后对流参数化方程组才是闭合的，这可以通过闭合假设来实现，即经验性地将云底质量通量与从观测场获得的观测变量相联系从而实现假设。

2.2.1 水汽辐合闭合

Tiedtke[5]将低层水汽辐合与云底质量通量相关联。其假设通过大尺度水平辐合和表层湍流通量而得到的云下层水汽供给，被通过云底的对流输送耗散

$$\left[M_u(q_u-\overline{q})+M_d(q_d-\overline{q})\right]_{z=z_b}=-\int_0^{z_b}\left[\overline{\boldsymbol{v}}\cdot\nabla\overline{q}+\overline{w}\frac{\partial\overline{q}}{\partial z}\right]\overline{\rho}\mathrm{d}z+(\overline{\rho}\overline{w'q'})_{tur} \quad (32)$$

式中右侧的最后一项表示表层湍流水汽通量。

2.2.2 对流有效位能闭合

Zhang等[9]用对流有效位能（CAPE）作为闭合。因为对流活动造成的大尺度温度和湿度在云层和云下层的变化与云底质量通量线性相关，由对流运动引起的*CAPE*变化可表示为

$$\left(\frac{\partial CAPE}{\partial t}\right)_{cu}=-M_bK \quad (33)$$

式中，K是对流单位云底上升气流质量通量的*CAPE*耗散率，它取决于大尺度热力学廓线和云模式。实际操作中是通过计算单位云底质量通量对模式*CAPE*的耗减来得到K。方程的闭合条件为对流造成*CAPE*以调整时间尺度为τ的指数速率消耗。因此有

$$M_b=\frac{CAPE}{\tau K} \quad (34)$$

通常其中的τ为数小时。这类闭合已在NCAR CAM[9]、ECMWF集成预报系统[33]和哈德莱中心HadAM3气候模式[34]中得以应用。基于CAPE闭合的一些其他形式也运用在Emanuel方案[7]和Kain-Fritsch方案中[35]。

2.2.3 准平衡闭合

Arakawa-Schubert（A-S）参数化方案通过一个准平衡假设实现闭合，此假设认为对流造成的大气稳定与大气大尺度过程造成的不稳定呈现准平衡。Arakawa-Schubert引入“云功函数”，它与CAPE相似但考虑了夹卷过程。因为Arakawa-Schubert方案采用云谱模式，每一子云型均为准平衡闭合

$$\frac{\mathrm{d}A_c(\lambda)}{\mathrm{d}t}=-\frac{\mathrm{d}A_{ls}(\lambda)}{\mathrm{d}t}\approx-\frac{A_{ls}^{t+\Delta t}(\lambda)-A^{t-\Delta t}(\lambda)}{2\Delta t} \quad (35)$$

式中，$\mathrm{d}A_c(\lambda)/\mathrm{d}t$和$\mathrm{d}A_{ls}(\lambda)/\mathrm{d}t$分别是由对流和大尺度过程所造成的云功函数随时间的变化率。$A_{ls}^{t+\Delta t}(\lambda)$是大尺度强迫后在时间点$t$的云功函数，$A^{t-\Delta t}$是观测的在$t-\Delta t$时的云功函数（对流发生后），$\Delta t$是观测的时间间隔。

在GCMs中应用A-S方案时，将Lord[26]得到的气候

值作为观测的云功函数，因此式（35）可写为

$$\frac{\mathrm{d}A_c(\lambda)}{\mathrm{d}t} \approx -\frac{A_{ls}^{t+\Delta t}(\lambda)-A_0(\lambda)}{2\Delta t} \qquad (36)$$

与CAPE闭合相似，由对流活动造成的云功函数的变化与云底质量通量成正比

$$\frac{\mathrm{d}A_c(\lambda)}{\mathrm{d}t} = -K(\lambda)m_b(\lambda) \qquad (37)$$

$K(\lambda)$可通过大尺度状况和云谱模式的计算获得，因而闭合方程变为

$$m_b(\lambda) = \frac{1}{K(\lambda)}\frac{A_{ls}^{t+\Delta t}(\lambda)-A_0(\lambda)}{2\Delta t} \qquad (38)$$

除了采用了云功函数并用于各云型，式（38）与CAPE闭合相似。

2.2.4 自由对流层准平衡闭合

Zhang[36-37]利用中纬度陆地对流和热带海洋对流资料对A-S准平衡再次加以研究，发现A-S准平衡闭合对上述两种情形都不适用。他引入自由对流层准平衡作为A-S准平衡的改进。由于CAPE是气块虚温与环境空气虚温间之差的垂直积分，CAPE（下文简记为A）随时间的变化可以是气块虚温变化的结果也可以是环境虚温变化的结果，即

$$\frac{\mathrm{d}A}{\mathrm{d}t} = \frac{\mathrm{d}A_p}{\mathrm{d}t} + \frac{\mathrm{d}A_e}{\mathrm{d}t} \qquad (39)$$

式中，下标p表示气块，下标e表示环境空气。Zhang[36]发现*CAPE*的变化很大程度上受控于气块虚温的变化，也就是说$\frac{\mathrm{d}A_e}{\mathrm{d}t}\approx 0$与云功函数相同，环境空气对*CAPE*变化的影响源于两类过程，对流过程和大尺度过程

$$\frac{\mathrm{d}A_e}{\mathrm{d}t} = \left(\frac{\mathrm{d}A_e}{\mathrm{d}t}\right)_c + \left(\frac{\mathrm{d}A_e}{\mathrm{d}t}\right)_{ls} \approx 0 \qquad (40)$$

式（40）构成了自由对流层准平衡的基础，它表明对流运动对自由对流层*CAPE*变化的影响与大尺度运动的影响相当。对对流云底质量通量的估算可用与A-S方案[式（36）～（38）]中云底质量通量估算相近的方法获得。

2.2.5 预测型闭合

以上所述闭合条件都是诊断性的，诊断性闭合的严重不足使其不能对对流运动的历史予以考虑。Pan等[38]在A-S对流参数化方案框架下开发了一个预测闭合。它不再假设对流和大尺度过程间的准平衡，而是预测整个气柱的次网格涡动动能，假定其与对流环流有关

$$\frac{\partial K}{\partial t} = AM_b - \frac{K}{\tau_D} \qquad (41)$$

式中，$K=\frac{1}{2}\int_{Z_s}^{Z_t}\rho(\overline{u'^2}+\overline{v'^2}+\overline{w'^2})$是地面到云顶的总涡动动能，$A$是云功函数，$M_b$是云底质量通量，$\tau_D$是一个可调参数，表示涡动动能的耗散时间尺度。Pan等[38]进一步通过下列假设将K与M_b联系起来

$$K = \alpha M_b^2 \qquad (42)$$

式中，α是另一个可调参数。式（41）和（42）形成了预测闭合，对云底质量通量进行预测。尽管预测闭合具有能对对流历史加以考虑的诱人之处，但相关研究直到近年才有了一定的进展。Chikira等[39]通过将预测闭合与修订的夹卷公式相结合对A-S方案进行了改进。Chikira[40]指出改进的A-S方案真实地模拟了许多全球气候的气候特点。

2.2.6 示例

图3展示不同闭合条件的准确性，图3a是运用式（36）计算的总*CAPE*变化的散点图，图3b是采用式（40）计算的*CAPE*变化的散点图。资料来自1997年6月19日－7月18日美国能源部大气辐射测量计划在美国中部南大平原的外场试验。斜率为－1的直线分别在图中对应A-S严格准平衡和自由对流层准平衡。尽管基于A-S闭合的对流诊断*CAPE*总变化总体与大尺度

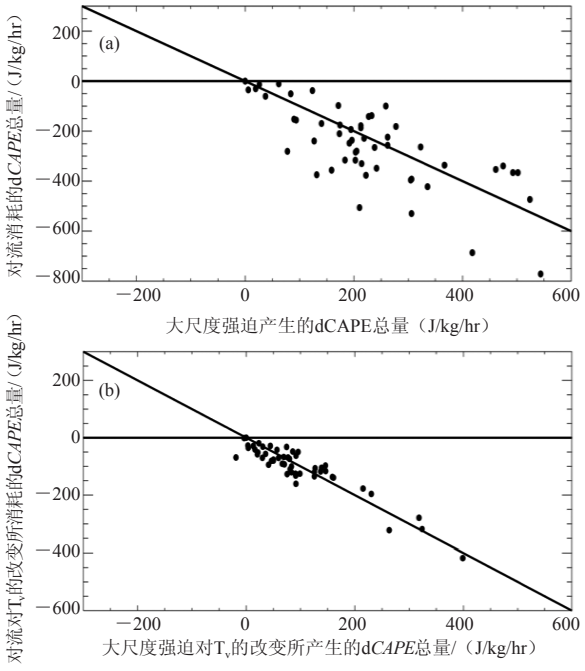

图3 中纬度对流环境下准平衡的散点图[37]
（a）A–S准平衡，（b）自由对流层准平衡（每个点代表3h平均;横坐标为大尺度强迫引起的*CAPE*变化，纵坐标为对流造成的*CAPE*变化）

Fig.3 Scatter plots demonstrating the validity of the A–S quasi–equilibrium assumption (top) and the free tropospheric quasi–equilibrium (bottom) in a midlatitude convection environment[37] (Each point represents a 3 h average, the x–axis is the *CAPE* change due to the large–scale forcing, and the y–axis is the *CAPE* change due to convection)

运动造成的总*CAPE*相关，但有较大的离散度，而用自由对流层准平衡闭合计算的对流造成的*CAPE*变化与大尺度强迫造成的*CAPE*变化的相关度要高得多。

自由对流层准平衡闭合已经在NCAR CAM3上测试，在热带气候模拟方面迄今已有大量重要进展，包括MJO和热带辐合带的模拟[41-43]。图4展示了MJO模拟的改进。径相合成剖面图显示模拟的MJO特征。10°S—10°N区域平均的850hPa纬向风、降水和向外长波辐射分别是用观测资料、采用对流参数化方案中的自由对流层准平衡闭合的CAM3模拟和标准的（基于CAPE）CAM3模拟。位相1、5、9分别对应于MJO周期的开始、成熟及结束阶段。采用观测资料的剖面图非常清楚地显示出在850hPa纬向风、降水和向外长波辐射中MJOs向东传播的特征，采用自由对流层准平衡闭合的CAM3模拟在三个方面都很好地模拟出了MJO向东传播的特征，振幅也相当。而标准的CAM3的模拟，尽管能隐约地显示出向东传播，但MJO信号都非常弱。

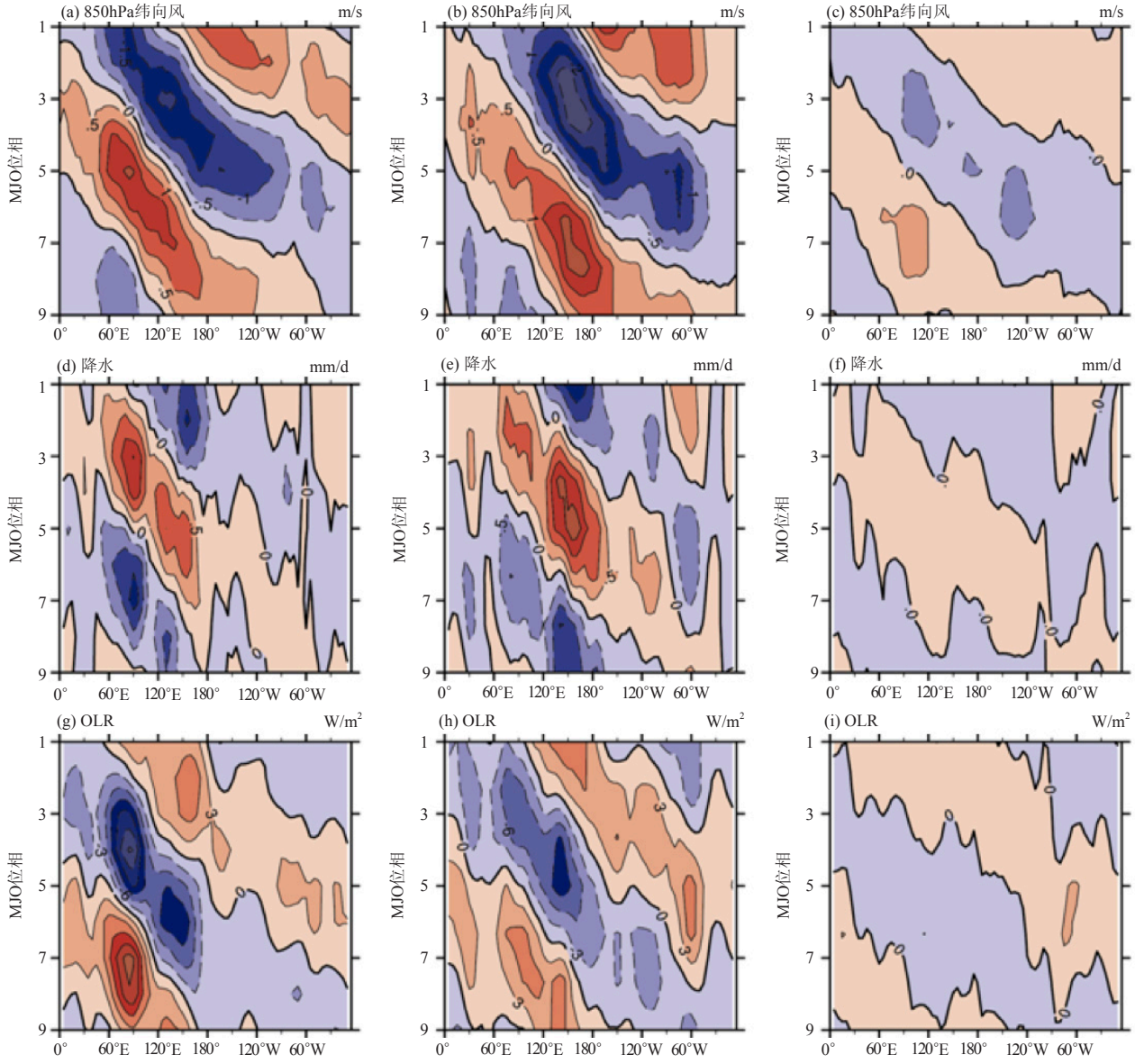

图4 MJO周期中850hPa纬向风（a，b，c）、降水（d，e，f）、向外长波辐射（g，h，i）位相–经度合成图（a，d，g）NCEP再分析／Xie—Arkin观测；（b，e，h）使用自由对流层准平衡的CAM3模拟，（c，f，i）使用CAPE的标准CAM3模拟

Fig.4 Phase–longitude plots of 850hPa zonal wind, precipitation and outgoing longwave radiation for a composite MJO cycle from (a, d, g) NCEP reanalysis/Xie–Arkin observations, (b, e, h) CAM3 new simulation, and (c, f, i) CAM3 control simulation, respectively

3 对流动量输送参数化

对流运动不仅输送热量和水分还输送动量。早在20世纪70年代 Austin等[44]通过收支分析就发现如果不考虑对流对动量的输送，地球的角动量无法平衡。之后，Schneider等[45]提出了对流动量输送（convective momentum transport，CMT）参数化方案。与热力学参数化相近，对流运动对动量的大尺度效应可表示为

$$\begin{aligned}\boldsymbol{X} &\equiv \frac{\partial \overline{\boldsymbol{v}}}{\partial t}+\overline{\boldsymbol{v}}\cdot\nabla\overline{\boldsymbol{v}}+\overline{\omega}\frac{\partial \overline{\boldsymbol{v}}}{\partial p}+\nabla\overline{\phi}+f\boldsymbol{k}\times\overline{\boldsymbol{v}}=-\nabla\cdot\overline{\boldsymbol{v}'\boldsymbol{v}'}-\frac{\partial\overline{\boldsymbol{v}'\omega'}}{\partial p} \\ &\simeq g\frac{\partial M_c(\boldsymbol{v}_c-\overline{\boldsymbol{v}})}{\partial p}\simeq -\frac{\partial M_c(\boldsymbol{v}_c-\overline{\boldsymbol{v}})}{\rho\partial z}\end{aligned} \quad (43)$$

式中，M_c是云质量通量，$\boldsymbol{v}_c$是云内空气的水平动量。这其中的难点在于确定云的平均动量。不同于像湿静力能这样的热力学变量，由于对流引发的云中气压梯度力的作用，即使在未稀释的上升气流中动量也是不守恒的。

由对流引发的气压梯度力通过作用于云平均动量$\boldsymbol{v}_c$而影响视动量源X。对于定常态云，对流云中的动量方程近似为

$$D\boldsymbol{v}_c-E\overline{\boldsymbol{v}}+\frac{\partial(M_c\boldsymbol{v}_c)}{\rho\partial z}=-\frac{1}{\rho}\sigma_c(\nabla p)_c \quad (44)$$

式中E和D是云边界处的质量卷入和卷出，并满足质量连续方程

$$\frac{\partial M_c}{\rho\partial z}=E-D$$

将以上代入动量源方程可得

$$\boldsymbol{X}=M_c\frac{\partial\overline{\boldsymbol{v}}}{\rho\partial z}+D(\boldsymbol{v}_c-\overline{\boldsymbol{v}})+\frac{1}{\rho}\sigma_c(\nabla p)_c \quad (45)$$

式中，第一项为上升气流质量通量和垂直风切变的乘积，它常被解释为云外环境补偿下沉造成的垂直平流。第二项是从对流上升气流到环境空气的水平动量卷出。最后一项是云区平均气压梯度。Schneider等[45]忽略了该对流气压效应。

20世纪80年代对流风暴的观测结果发现对流活动能在风暴场中和风暴周围产生很大的气压扰动，这能对云内的水平动量起到调制作用[46-47]。为体现这一扰动气压场的效应，Zhang等[10-11]由一个三维动量方程开始

$$\rho\frac{\partial\boldsymbol{v}_3}{\partial t}+\rho\boldsymbol{v}_3\cdot\nabla_3\boldsymbol{v}_3+2\rho\boldsymbol{\Omega}\times\boldsymbol{v}_3=-\nabla p+\boldsymbol{k}\rho B \quad (46)$$

式中，$\boldsymbol{v}_3=(u,v,w)$是三维风向量，$\boldsymbol{\Omega}$是科里奥利参数的向量形式，B是云团浮力。我们注意到$\boldsymbol{v}_3\cdot\nabla_3\boldsymbol{v}_3+2\boldsymbol{\Omega}\times\boldsymbol{v}_3=\nabla_3(\frac{1}{2}\boldsymbol{v}_3\cdot\boldsymbol{v}_3)+\boldsymbol{\eta}\times\boldsymbol{v}_3$，而$\boldsymbol{\eta}=\nabla_3\times\boldsymbol{v}_3+2\boldsymbol{\Omega}$是三维绝对涡度。将三维散度运算代入三维动量方程并运用质量连续方程，得到

$$\begin{aligned}\nabla_3^2p&=-\nabla_3\left(\frac{\rho}{2}\nabla_3\boldsymbol{v}_3\cdot\boldsymbol{v}_3\right)-\nabla_3\cdot\left(\rho\boldsymbol{\eta}\times\boldsymbol{v}_3\right)+\nabla_3\cdot(\rho\boldsymbol{k}B) \\ &=-\nabla_3^2\left(\frac{\rho}{2}\boldsymbol{v}_3\cdot\boldsymbol{v}_3\right)+\nabla_3\cdot\left(\frac{1}{2}\boldsymbol{v}_3\cdot\boldsymbol{v}_3\nabla_3\rho\right)+\rho\eta^2+\boldsymbol{v}_3\cdot\left(\nabla_3\times\rho\boldsymbol{\eta}\right)+\nabla_3\cdot(\rho\boldsymbol{k}B)\end{aligned} \quad (47)$$

浮力对垂直气压梯度的产生很重要，它对对流云区的水平气压梯度的影响依赖于云的倾斜度[46]，鉴于对此了解不多，在CMT参数化方案中被略去。

将式（47）展开得

$$\nabla_3^2p=-2\rho\left[\frac{\partial w}{\partial x}\frac{\partial u}{\partial z}+\frac{\partial w}{\partial y}\frac{\partial v}{\partial z}+\frac{\partial v}{\partial x}\frac{\partial u}{\partial y}\right]-\rho\left[(\frac{\partial u}{\partial x})^2+(\frac{\partial v}{\partial y})^2+(\frac{\partial w}{\partial z})^2\right]+w^2\rho\frac{\partial}{\partial z}\left(\frac{1}{\rho}\frac{\partial\rho}{\partial z}\right) \quad (48a)$$

Zhang等[10-11]用付里叶函数和贝塞尔函数展开，加上适当的边界条件求解式（48a）得到云中气压梯度。Zhang等[48]评估了CMT对气候模拟的影响，发现其对气候平均态影响很大。后来的研究发现CMT对厄尔尼诺和MJO的模拟也有作用[49-50]。

在Zhang等[10-11]的工作之后，研究人员一直在探索扰动气压梯度力的简化表达形式。考虑对流垂直速度和扰动气压的水平变化具有谐波形式，可以得到简化表达式。式（48a）的右端项可分成线性和非线性两部分

$$\begin{aligned}\nabla_3^2p=&-2\rho\frac{\partial w}{\partial x}\frac{\partial\overline{u}}{\partial z}-2\rho\frac{\partial w}{\partial y}\frac{\partial\overline{v}}{\partial z}-2\rho\frac{\partial w}{\partial x}\frac{\partial u'}{\partial z}-2\rho\frac{\partial w}{\partial y}\frac{\partial v'}{\partial z} \\ &-\rho\left[(\frac{\partial u}{\partial x})^2+(\frac{\partial v}{\partial y})^2+(\frac{\partial w}{\partial z})^2\right]+w^2\rho\frac{\partial}{\partial z}\left(\frac{1}{\rho}\frac{\partial\rho}{\partial z}\right)\end{aligned} \quad (48b)$$

式中，右端前两项是对扰动气压场的线性强迫，与平均风的垂直切变成正比，其余项代表非线性强迫，其中第一项与扰动风切变相关，方括号中内容与辐散流相关，而最后一项与大气层结相关。若仅考虑线性强迫

$$\nabla_3^2p\approx-2\rho\frac{\partial w}{\partial x}\frac{\partial\overline{u}}{\partial z}-2\rho\frac{\partial w}{\partial y}\frac{\partial\overline{v}}{\partial z}$$

假设w为正弦形式

$$w = w_0 \cos kx \cos ly \sin mz,\quad -\frac{\pi}{2} < kx, ly < \frac{\pi}{2}$$

式中，k，l和m分别是x，y和z方向上的波数，则

$$p = \frac{2\rho}{k^2+l^2+m^2}\left(\frac{\partial \overline{u}}{\partial z} k \sin kx \cos ly + \frac{\partial \overline{v}}{\partial z} l \cos kx \sin ly\right) w_0 \sin mz$$

$$\frac{1}{\rho}\frac{\partial p}{\partial x} = \frac{2w_0}{k^2+l^2+m^2}\left(\frac{\partial \overline{u}}{\partial z} k^2 \cos kx \cos ly - \frac{\partial \overline{v}}{\partial z} kl \sin kx \sin ly\right) \sin mz$$

$$\frac{1}{\rho}\frac{\partial p}{\partial y} = \frac{2w_0}{k^2+l^2+m^2}\left(-\frac{\partial \overline{u}}{\partial z} kl \sin kx \sin ly + \frac{\partial \overline{v}}{\partial z} l^2 \cos kx \cos ly\right) \sin mz$$

在云中平均可得

$$\frac{\sigma_c}{\rho}\left(\frac{\partial p}{\partial x}\right)_c = -\frac{2k^2}{k^2+l^2+m^2}\frac{\partial \overline{u}}{\partial z}\sigma_c w_c = -\gamma_x M_c \frac{\partial \overline{u}}{\rho \partial z} \quad (49a)$$

$$\frac{\sigma_c}{\rho}\left(\frac{\partial p}{\partial y}\right)_c = -\frac{2l^2}{k^2+l^2+m^2}\frac{\partial \overline{v}}{\partial z}\sigma_c w_c = -\gamma_y M_c \frac{\partial \overline{v}}{\rho \partial z} \quad (49b)$$

式中，γ_x和γ_y是取决于对流云水平和垂直尺度的系数，因此，对流引发的压力梯度除了取决于对流上升气流的质量通量和风切变，还取决于对流上升气流的水平和垂直尺度。对于在水平和垂直方向上有相同尺度的对流上升气流，则$k=l=m$，$\gamma_x=\gamma_y=0.67$。

Wu等[12]首先采用了这一方法，之后Gregory等[13]用云分辨模式模拟来估算这一参数，并发现$\gamma=0.7$是一个很好的近似。利用云分辨模式对TOGA COARE对流的模拟，Zhang等[51]也估算了CMT中对流气压梯度力的作用，发现$\gamma=0.5$与模式结果更一致。将式（49）代入方程（45），得

$$\boldsymbol{X} = (1-\gamma)M_c \frac{\partial \overline{\boldsymbol{v}}}{\rho \partial z} + \delta(\boldsymbol{v}_c - \overline{\boldsymbol{v}}) \quad (50)$$

图5显示Zhang等[51]得到的对流上升气流平均气压梯度力的x分量和对流对CMT的效应，也称为视动量源。Zhang等[10-11]研究中通过求解扰动气压方程得到的云平均气压梯度力与模式模拟结果非常吻合。取$\gamma=0.55$通过式（49）得到的最小二乘法拟合也有很好的吻合度。尽管量级有些偏大，但视动量源参数化抓住了模拟CMT的最重要特征。

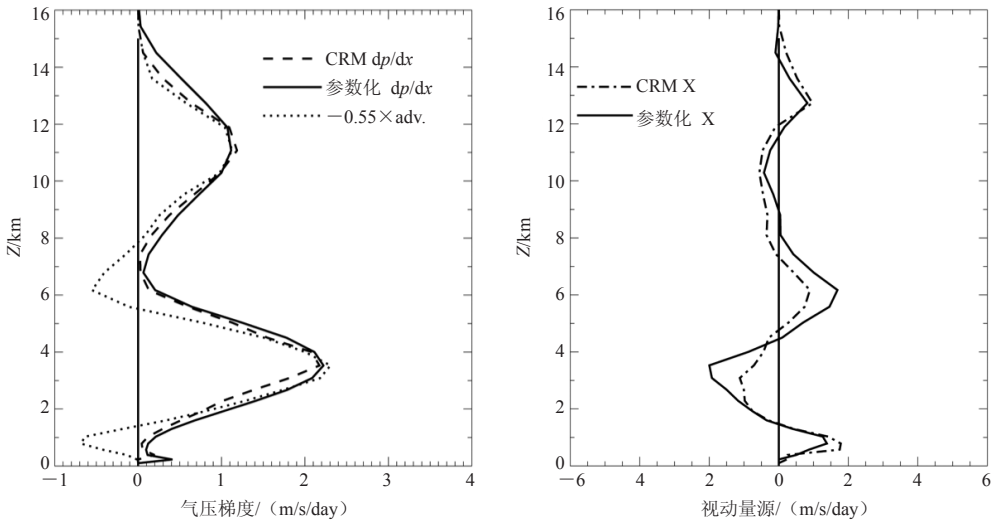

图5 模拟和参数化得到的气压梯度和视动量源垂直廓线[51]

[对气压梯度，虚线来自云模式模拟；实线来自Zhang等[10−11]的参数化；点线来自式（47），取常系数−0.55。对视动量源，虚点线来自模拟，实线来自参数化]

Fig.5 Vertical profiles of time average pressure gradient and apparent momentum source from parameterizations and model simulation[51]

[For pressure gradient, dashed line is from model simulation, solid line is from Zhang and Cho's parameterization, and dotted line is from Eq. (47) with a constant coefficient of −0.55; for apparent momentum source, dash−dotted line is from model simulation, and solid line is from Zhang and Cho's parameterization]

4 讨论与结论

本文综述的很多对流参数化方案广泛应用于全球预报和气候模式中。Tiedtke方案用于欧洲中期预报中心的业务模式中[52]，Emanuel方案在美国海军业务全球大气预报系统中使用[53]，Zhang等方案应用于NCAR CAM模式中[41-42]，Arakawa等方案用于美国国家环境预测中心模式中[54]。尽管对流参数化方案在模式中的表现取决于多种因素，目前已有的参数化方案的一些共同弱点也是众所周知的，如赤道双辐合带、弱MJO、错误的对流日变化、弱降水太频繁和缺少强降水等。这些都表明对流参数化需要进一步改进，近年来在这方面有些新的发展。

如前文所述，对对流上升气流内微物理过程的处理是近年令人关注的研究点，因为对流云中卷出的水物质是大尺度云发展中云水和冰的重要来源。另外，减小气溶胶—对流相互作用和气溶胶对云的间接效应中的不确定性要求对流微物理过程的参数化更为精确。文献[14-17]的工作为我们在此方向上开辟了新的研究途径。

在“超级参数化”或所谓的多尺度建模框架（multi-scale modeling framework，MMF）方面也有重要进展，它通过在GCM中嵌入云系统分辨模式代替传统的对流参数化[55-57]。此方法通常比传统对流参数化方案[58]模拟结果更好，但计算量很大。对于气候预估研究，需要数百年甚至上千年数据的集合模拟，此方法至少在未来十年中不可行。然而即使这一方法无法在可预见的未来代替对流参数化，它仍是评估和推进传统对流参数化方案的极好工具。

当今对流参数化面临的一个主要问题是其对分辨率的依赖性。在未来五至十年，数值天气预报模式分辨率有望达到5km甚至更高，而GCM分辨率有望达到10km，在这些分辨率下，网格尺度运动和深对流运动的区分将不再清晰。那目前的对流参数化方案在什么范围内仍将适用呢？如前所述[式（14）和（15）]，所有的对流参数化方案都假设在模式网格中对流云量远远小于1，这一假设在模式格距为100km或者更大时通常是适用的，但是当模式格距减小为10km或更小时则不能成立。在如此高分辨率下，对流云量很容易就达到0.5甚至更大，因而对流参数化方案也需要重新开发。近期，Arakawa等[59-60]研究了在不能忽略云量的情况下重新设计对流参数化方案的可能性。他们认为通过额外引入一个方程来代替云量，现有的参数化方案经修改可以用于高分辨率数值模式。此类研究目前处于初期，还需要做大量的工作为高分辨率数值模式中对流参数化方案提供坚实基础。

另一个面临的问题是确定对流云，特别是上升气流的垂直速度。上升气流垂直速度对于包括云滴活化和气溶胶冰成核过程的对流微物理过程十分重要，在给定上升气流质量通量时上升气流垂直速度也可用来确定对流云量。另外，近期对对流参数化中卷出估算的研究也需要对上升气流垂直速度的了解。

最后，次网格尺度变化和对流初生的触发条件也是对流参数化的重要问题。当前在对流参数化方案中是利用网格平均属性来诊断对流活动，而现实中，对流上升气流与诸如冷池流/阵风锋和暖泡等局地次网格特征密切相关，而对流初期的触发条件决定对流何时发生。全球气候模式对对流日循环错误的模拟很可能与不恰当的对流触发函数相关。然而，现今的对流参数化方案中所有的触发函数的设计均存在太大的任意性，没有用观测资料或云模式模拟结果进行系统评估。研究[52,54]表明触发函数对气候模拟有重要影响，因此对触发函数进行更多的系统评估无疑是十分需要的。

本文旨在对气候和数值天气预报模式中广泛应用的对流参数化方案给予全面评述，重点是质量通量型方案。用一个一维定常态云模式展示了其在确定对流参数化方案所需云特性中的作用。也扼要地讨论了随机混合模式。对数个闭合条件予以描述以反映目前业界对此问题的理解。通过一节描述了对流动量输送参数化，对流动量输送参数化的难点在于估算对流引发的扰动气压梯度力的效应。文中还对目前对流参数化方案研究和全球气候模拟、数值天气预报界面临的一些突出问题进行了简要阐述。

致谢：感谢NOAA地球物理流体动力实验室（GFDL）Leo Donner博士多年来和作者就对流参数化问题进行有益的讨论。

（译者：王卫丹，中国气象局气象干部培训学院）

Mass-Flux-Based Parameterization of Atmospheric Convection in Weather and Climate Models

Zhang Guangjun [1, 2]

(1 Center for Earth System Science, Tsinghua University, Beijing 100084
2 Scripps Institution of Oceanography La Jolla, USA)

Introduction

The representation or parameterization of atmospheric convection in numerical models has been a challenging task ever since the dawn of the numerical weather prediction and climate modeling era. Individual convective cells have small spatial and temporal scales, on the order of less than a kilometer to a few tens of kilometers in space, and a few minutes to a few hours in time. Organized convective systems, such as squall lines and mesoscale convective complexes could be several hundred kilometers in size and last over a day or longer. Convection is an important energy source for atmospheric circulation, particularly in the tropics. From a socioeconomic point of view, convection is often associated with high impact, extreme weather, such as flashflood, tornadoes, and hurricanes/typhoons, which can cause high economic tolls on society. Thus, accurate forecast of convection or severe storms, in both timing and location, is of paramount importance to numerical weather prediction. Because of its small spatial-scale, convection cannot be resolved by global climate models (General Circulation Models, GCMs) and numerical weather prediction (Numerical Weather Prediction, NWP) models, and thus has to be parameterized.

The parameterization of the vertical transport of mass, heat and moisture by atmospheric convection has always been an extremely difficult problem since convection strongly interacts with clouds, atmospheric water vapor and radiation, involving processes operative at space and time scales spanning several orders of magnitudes. Over the past half century, many parameterization schemes have been developed, from simple convective adjustment schemes[1-2] to moisture-convergence-based[3-5] and convective-instability-based mass flux schemes[6-9]. As our understanding of convection and its interaction with large-scale circulation and clouds deepens, more physical processes are included in convection parameterization, including convective transport of momentum[10-13] and convective cloud microphysical processes[14-17]. From the climate change research perspective, clouds and aerosols are two of the most important factors contributing to the uncertainty in climate change projection[18]. Both are closely tied to convection. In the tropics, clouds are often convectively generated. Detrainment of cloud ice and liquid water forms the anvil clouds that have a tremendous impact on the Earth's radiation budget. Aerosols not only have a direct effect on atmospheric radiation, they also serve as cloud condensation and ice nuclei. Convection can transport aerosols vertically; scavenging and washout by rainfall can also affect aerosol loading in the atmosphere. Recent observations also indicate that aerosols can have a significant impact on convection[19-20].

This paper will provide a comprehensive review of the development of convective parameterization. We will concentrate on deep, precipitating atmospheric convection. Section 1 will briefly introduce the early development of convective parameterization. Section 2 will review a number of mass flux based convective parameterization schemes. In section 3, the parameterization of convective momentum transport will be reviewed. Section 4 will discuss recent progress and remaining outstanding issues, followed by a few concluding remarks.

1. Convection parameterization in the early days

The role of convective heating in large-scale circulation was already recognized in the early days of global climate modeling. Manabe et al.[1] was among the first to include it in the Geophysical Fluid Dynamics Laboratory (Geophysical Fluid Dynamics Laboratory, GFDL) model through convective adjustment. The idea and approach were simple and practical: in a layer of the atmosphere if the vertical lapse rate of temperature exceeds neutral stratification, adjustment will take place instantly to remove the instability. For unsaturated atmosphere, this is achieved through dry adjustment by requiring

if

$$-\frac{\partial T}{\partial p} > \gamma_d$$

$$\begin{aligned} &\delta q = 0 \\ &\frac{\partial}{\partial p}\theta(T+\delta T, p) = 0 \\ &\int_{p_B}^{p_T} \delta T \mathrm{d}p = 0 \end{aligned} \tag{1}$$

where γ_d is dry adiabatic lapse rate, δq is adjustment of water vapor mixing ratio, δT is temperature adjustment, θ potential temperature, P_T and P_B are pressure at the top and bottom of the atmospheric layer where dry adjustment is required. The temperature adjustment at each model level is obtained by solving Eq. (1). Similarly, for saturated air, moist adjustment over a layer is performed by satisfying the following set of equations:

if

$$-\frac{\partial T}{\partial p} > \gamma_m$$

$$\begin{aligned} &\frac{\partial}{\partial p}\theta_e(T+\delta T, q+\delta q, p) = 0 \\ &q+\delta q = q_s(T+\delta T, p) \\ &\int_{p_B}^{p_T} c_p \delta T + L\delta q \mathrm{d}p = 0 \end{aligned} \tag{2}$$

where θ_e is equivalent potential temperature, q_s is saturation water vapor mixing ratio, c_p and L are specific heat at constant pressure and latent heat of condensation, respectively. δT and δq are obtained by solving Eq. (2). Although simple, this adjustment approach accounts for the most essential effect of subgrid-scale convection, heating of the atmosphere and depletion of moisture in the convecting layer.

At the same time, in an effort to incorporate the effect of convection in hurricane modeling, Kuo[3-4] developed a convection parameterization scheme, recognizing that deep convection cells are "hot towers"[21] transporting warm and moist surface air to the upper troposphere. Kuo[3-4] introduced a cloud model, in which latent heat release from convection is achieved through vertical motion inside the cloud, instead of through local adjustment as done by Manabe et al.[1]. Convection collectively affects the grid-scale temperature through mixing of warm cloud air with its environment.

The Kuo[3-4] scheme assumes that (1) convection occurs in a region where the atmosphere is conditionally unstable and there is low-level moisture convergence; (2) convective clouds originate from the boundary layer and the cloud temperature and moisture profiles can be characterized by a pseudo-moist adiabat typical of the boundary layer air; and (3) clouds extend from the lifting condensation level of the boundary layer air to the neutral buoyancy level of this air. A key parameter in the scheme is the amount of precipitation, through which the net condensational heating in the atmospheric column can be estimated. With the above assumptions, the Kuo scheme starts with the large-scale moisture equation integrated over the atmospheric column:

$$\int_0^{p_s} \frac{\partial \overline{q}}{\partial t}\mathrm{d}p = -P g - \int_0^{p_s} \nabla\cdot(\overline{v}\,\overline{q})\mathrm{d}p + gF_{LH} = g(M_t - P) \tag{3}$$

where

$$M_t = -\frac{1}{g}\int_0^{p_s} \nabla\cdot(\overline{v}\,\overline{q})\mathrm{d}p + F_{LH} \tag{4}$$

is the total moisture supply to the atmospheric column including lateral convergence and surface evaporation F_{LH}. P is precipitation on the surface, which equals the column integral of the net condensation:

$$P = \frac{1}{g}\int_0^{p_s}(c-e)\mathrm{d}p \tag{5}$$

The overbar denotes large-scale average. Kuo[3-4] assumed that a small fraction of the moisture supply (bM_t) is used to moisten the atmosphere and the rest is precipitated out as rain, i.e.

$$P = (1-b)M_t \tag{6}$$

where b is a tunable parameter. Thus, knowing the total moisture supply M_t, which can be computed from the large-scale or grid-scale fields, one can compute the surface precipitation P, or the vertical integral of latent heating. Since Eqs. (3)–(6) are given in the form of vertical integral over the atmospheric column, the vertical distribution of heating must be specified in order to determine the effect of convection on temperature field at each model level. Kuo[3-4] further assumed that the condensational heating is proportional to the temperature difference between the cloud air following a pseudo-moist adiabat and the environmental air. This gives

$$L(c-e) = \frac{gLP}{p_b - p_t}\frac{T_c - \overline{T}}{< T_c - \overline{T} >} \tag{7}$$

where the angle brackets represent the vertical average over the cloud layer. p_b and p_t are the pressure levels of the cloud base and cloud top, respectively. Outside the cloud layer latent heating is zero.

In the late 1960s and early 70s, other groups of researchers also engaged in active research on convection parameterization[22-23]. Instead of resorting to the concept of mixing between cloudy air and environmental air to heat the large-scale atmosphere, they introduced the concept of compensatory subsidence. Under this

framework, convective updrafts transport air mass from the surface to the upper troposphere. By mass continuity, the compensating subsidence takes place in the convection environment, thereby adiabatically heating the ambient atmosphere. Kuo (1974) showed that the mechanisms of convective heating of the atmosphere between his approach and the mass-flux-based thinking are equivalent although the interpretation may differ.

A major weakness of the Kuo scheme is that it has no ability to predict the moisture field by assuming that a certain fraction b of moisture convergence is used to moisten the atmosphere. Because of this weakness, it has not been widely used in numerical models although the one that did use it seemed to be quite successful[24].

2. Mass-flux-based parameterization

The most comprehensive, classic work on convection parameterization to date was by Arakawa et al. [6]. It established the foundation for most of the mass-flux-based convective parameterization schemes used today in numerical weather prediction and global climate models. Thus, we will devote some space to this type of schemes in this section. Typically convection parameterization assumes that convection occurs on spatial scales of a few kilometers or less and is of subgrid scale to model resolutions. The governing equations for the large-scale temperature and moisture fields can be written as[25].

$$\frac{\partial \overline{s}}{\partial t}+\nabla\cdot(\overline{\boldsymbol{v}}\,\overline{s})+\frac{\partial(\overline{\rho}\,\overline{w}\,\overline{s})}{\overline{\rho}\partial z}=\overline{Q}_R+L(c-e)-\nabla\cdot(\overline{\boldsymbol{v}'s'})-\frac{\partial\overline{\rho}\,\overline{w's'}}{\overline{\rho}\partial z} \quad (8)$$

$$\frac{\partial \overline{q}}{\partial t}+\nabla\cdot(\overline{\boldsymbol{v}}\,\overline{q})+\frac{\partial(\overline{\rho}\overline{w}\overline{q})}{\overline{\rho}\partial z}=-(c-e)-\nabla\cdot(\overline{\boldsymbol{v}'q'})-\frac{\partial\overline{\rho}\,\overline{w'q'}}{\overline{\rho}\partial z} \quad (9)$$

where $s=CpT+gz$ is the dry static energy, q is the specific humidity, v is the horizontal wind vector, w is the vertical velocity, and L is the latent heat of vaporization. The overbar represents average over the large-scale domain or a model grid box and the prime represents the deviation from the mean. The perturbation product terms on the right-hand side represent the effect of subgrid scale transport (i.e. convection) on the large-scale or grid mean fields. Q_R is the radiative heating rate. $c-e$ represents the net condensation (condensation minus evaporation) within the NWP model or GCM grid box. Note that we have neglected deposition/sublimation and heating from freezing/melting in Eqs. (8) and (9). Typically, the horizontal divergence of the perturbation flux is much smaller than the vertical divergence term and can be neglected. Thus, the convective effects on the large-scale temperature and moisture fields are:

$$\left(\frac{\partial\overline{T}}{\partial t}\right)_c=\left(L(c-e)-\frac{\partial\overline{\rho}\,\overline{w's'}}{\overline{\rho}\partial z}\right)\Big/C_p \quad (10)$$

$$\left(\frac{\partial\overline{q}}{\partial t}\right)_c=-(c-e)-\frac{\partial\overline{\rho}\,\overline{w'q'}}{\overline{\rho}\partial z} \quad (11)$$

To parameterize these effects in terms of large-scale variables, note that any variable x can be written as: $x=\overline{x}+x'$, where $\overline{x}=\frac{1}{A}\int x\mathrm{d}A$ is the average of x over area A, and $x'=x-\overline{x}$. Thus, $\overline{x'}=0$. Assuming that within this area there are a number of cumulus clouds occupying a total area A_c, and the convection free area is A-A_c (Fig. 1). The mean value of x in convective area is x_c and the mean value in convection free region is x_e. Then

$$\begin{aligned}\overline{x}&=(A_cx_c+(1-A_c)x_e)/A=\sigma x_c+(1-\sigma)x_e\\ x_c'&=x_c-\overline{x}=(1-\sigma)(x_c-x_e)\\ x_e'&=x_e-\overline{x}=-\sigma(x_c-x_e)=-\frac{\sigma}{1-\sigma}x_c'\end{aligned} \quad (12)$$

where $\sigma=A_c/A$ is the fractional area occupied by convective clouds. If we further assume that there is no correlation between x' and y' within clouds or the environment, and make use of Eq. (12), the eddy correlation of the product of two variables x and y can be written as:

$$\begin{aligned}\overline{x'y'}&=\sigma(x'y')_c+(1-\sigma)(x'y')_e=\sigma x_c'y_c'+(1-\sigma)x_e'y_e'\\ &=\sigma x_e'y_e'+(1-\sigma)(-\frac{\sigma}{1-\sigma}x_c')(-\frac{\sigma}{1-\sigma}y_c')=\frac{\sigma}{1-\sigma}x_e'y_e'\\ &=\frac{\sigma}{1-\sigma}(x_c-\overline{x})(y_c-\overline{y})\end{aligned} \quad (13)$$

For vertical transport of dry static energy s, let $y=s$ and $x=w$:

$$\overline{\rho}\overline{w's'}=\frac{\sigma}{1-\sigma}\overline{\rho}(w_c-\overline{w})(s_c-\overline{s}) \tag{14}$$

For numerical models such as current GCMs, the horizontal resolution is on the order of 100 km or larger and the fractional area occupied by convection is generally small, $\sigma \ll$ land $\overline{w} \ll w_c$. Thus Eq. (14) reduces to

$$\overline{\rho}\overline{w's'}\approx\sigma\overline{\rho}w_c(s_c-\overline{s})=M_c(s_c-\overline{s}) \tag{15a}$$

Here $M_c=\sigma\overline{\rho}w_c$ is convective cloud mass flux. If both updrafts and downdrafts are considered, the above equation should be written as:

$$\overline{\rho}\overline{w's'}=M_u(s_u-\overline{s})+M_d(s_d-\overline{s}) \tag{15b}$$

where subscripts u and d denote updrafts and downdrafts, respectively. For numerical weather prediction models or high-resolution global climate models, the model grid spacing can be as small as 10 km, and the fractional area occupied by convection is no longer negligible. In such cases, all terms in eq. (14) must be retained and the approximation Eqs. (15a) and (15b) will break down. This will be further discussed later.

With Eq. (15b), the large-scale temperature and moisture budget equations incorporating the effect of convection can be written as:

$$\frac{\partial\overline{s}}{\partial t}+\nabla\cdot(\overline{v}\,\overline{s})+\frac{\partial(\overline{\rho}\,\overline{w}\,\overline{s})}{\overline{\rho}\partial z}=\overline{Q}_R+L(c-e)-\frac{\partial}{\overline{\rho}\partial z}[M_u(s_u-\overline{s})+M_d(s_d-\overline{s})] \tag{16}$$

$$\frac{\partial\overline{q}}{\partial t}+\nabla\cdot(\overline{v}\,\overline{q})+\frac{\partial(\overline{\rho}\,\overline{w}\,\overline{q})}{\overline{\rho}\partial z}=-(c-e)-\frac{\partial}{\overline{\rho}\partial z}[M_u(q_u-\overline{q})+M_d(q_d-\overline{q})] \tag{17}$$

Eqs. (16) and (17) are the starting points of all mass-flux-based convection parameterization schemes. It is clear that to parameterize the convective effects on large-scale temperature and moisture fields, one needs to know the cloud mass flux, in-cloud temperature and moisture, as well as condensation and evaporation inside convective updrafts and downdrafts. This is accomplished through the introduction of simple updraft and downdraft models and closure assumptions.

2.1 Cloud models

2.1.1 Steady-state model

Updrafts and downdrafts in convective clouds are often considered as plumes of air mass. For parameterization purposes, a steady state is typically assumed for clouds. In this case, the bulk equation for an in-cloud property is in the form of

$$\frac{\partial F}{\rho\partial z}=\text{source}-\text{sink}$$

where F is the flux across the interface of a model layer. The source and sink within the layer are either generated inside the cloud or transported from the lateral boundary. For mass flux, heat, moisture and cloud condensate within updrafts, the equations are[9]:

$$\frac{\partial M_u}{\rho\partial z}=E_u-D_u \tag{18}$$

$$\frac{\partial M_u s_u}{\rho\partial z}=E_u\overline{s}-D_u\hat{s}_u+L(c-e) \tag{19}$$

$$\frac{\partial M_u q_u}{\rho\partial z}=E_u\overline{q}-D_u\hat{q}_u-(c-e) \tag{20}$$

$$\frac{\partial M_u l}{\rho\partial z}=-D_u l+(c-e)-R_r/\rho \tag{21}$$

where E_u and D_u are the mass entrainment and detrainment. s_u and q_u are dry static energy and specific humidity in the updrafts. Air within updrafts is assumed saturated:

$$q_u=q_s(s_u) \tag{22}$$

$\hat{s}_u$ and $\hat{q}_u$ are the dry static energy and moisture detrained into the environment. At the detrainment level, it is often assumed that the air has the same temperature as that of its environment and is saturated,

$$\hat{s}_u=\overline{s} \tag{23}$$

$$\hat{q}_u=q_s(\overline{s}) \tag{24}$$

In Eq. (21), the cloud liquid water detrained into the environment is assumed to be the same as the mean updraft liquid water content at that level. R_r is the conversion rate of cloud liquid water to rain, and is often assumed to be proportional to cloud water content l[5,6,9]. For example, Zhang and McFarlane[9] uses the following form based on Lord[26]:

$$R_r=c_0M_u l \tag{25}$$

with $c_0=2\times10^{-3}\text{m}^{-1}$. Note that freezing is not considered, thus l represents the total condensate in Eq. (21). In the National Center for Atmospheric Research (NCAR) Community Atmosphere Model version 5 (CAM5), where the Zhang-McFarlane scheme is used, the total condensate in updrafts is further partitioned into cloud water and ice based on temperature, with the extra latent heating from freezing for detrained ice added to the large-scale temperature equation.

In this simple steady-state 1-D model, cloud microphysics inside convective updrafts is very crudely parameterized through a tuning parameter in Eq. (25). A number of recent studies[19-20] have indicated that aerosols can have a significant effect on the convective cloud development. Representing aerosol effects on convection requires cloud microphysics in the convection parameterization. Furthermore, convective detrainment of cloud ice and water is an important source for large-scale or anvil clouds, which have fundamental impacts on the Earth's radiation budget. In view of the importance of aerosol-convection-cloud-radiation interaction, the overly simplified treatment of convective microphysics is no longer adequate. Recently, a few sophisticated convective microphysics schemes have been developed [14-17]. Interested readers are referred to these works.

The updraft mass flux in Eqs. (18)–(21) needs to be known and this is done through the specification of entrainment and detrainment. Tiedtke[5] partitioned the entrainment into organized inflow and turbulent entrainment, and the mass detrainment into organized outflow and turbulent detrainment:

$$E_u = E_u^1 + E_u^2 \,,\; D_u = D_u^1 + D_u^2 \tag{26}$$

where $E_u^1 = \varepsilon_u M_u$ and $D_u^1 = \delta_u M_u$ are turbulent entrainment and detrainment, respectively. The fractional entrainment/detrainment rates ε_u and δ_u are set to depend on cloud type. For shallow convection in convectively suppressed conditions, $\varepsilon_u = \delta_u = 3\times10^{-4}\mathrm{m}^{-1}$. For penetrative and mid-level convection in the presence of large-scale convergence, $\varepsilon_u = \delta_u = 1\times10^{-4}\mathrm{m}^{-1}$. The different values for shallow and deep convection are meant to mimic the fact that shallow convective clouds are smaller in size and thus are subject to more entrainment from the cloud boundaries, whereas deep convective clouds under disturbed conditions are large and are subject to less entrainment. For organized entrainment, in the case of deep convection Tiedtke[5] assumed it to be proportional to large-scale moisture convergence:

$$E_u^2 = -\frac{\overline{\rho}}{\overline{q}}\left(\overline{\boldsymbol{v}}\cdot\nabla\overline{q} + \overline{w}\frac{\partial\overline{q}}{\partial z}\right) \tag{27}$$

For shallow convection, no organized entrainment is present because these clouds often exist in regions of large-scale subsidence. Organized detrainment for deep convection is assumed to occur only at the highest cloud layer, where all convective mass flux is detrained. For shallow convection, organized detrainment is allowed to occur at the top most two cloud layers, with 70% of the mass flux detrained at the zero-buoyancy level and 30% detrained above it to represent overshooting into the inversion layer. With the mass entrainment and detrainment specified, Eqs. (18)–(25) can be integrated to obtain the cloud properties in convective updrafts.

In ensemble-plume-based models[6,9], only turbulent entrainment and organized detrainment are considered. The fractional entrainment rate is determined in a more complicated way. For each cloud type with fractional entrainment rate λ, the variation of mass flux with height is given by:

$$\frac{\partial m_u(\lambda,z)}{\partial z} = \lambda m_u(\lambda,z) \tag{28}$$

Integrating over all possible λ's that contribute to the mass flux at level z gives:

$$M_u(z) = \int_0^{\lambda_D(z)} m_u(\lambda,z)\mathrm{d}\lambda \tag{29}$$

where $\lambda_D(z)$ is the fractional entrainment rate of the updraft that detrains at height z. Here it is implicitly assumed that $\lambda_D(z)$ decreases monotonically with height. Thus, clouds with $\lambda > \lambda_D(z)$ have no contribution to mass flux at height z. The quantity λ_D is determined by the requirement that the temperature of the clouds detraining at height z is the same as that in its environment, which is ensured by requiring that

$$h_b - h^*(z) = \lambda_D(z)\int_{z_b}^{z}\left[h_u(\lambda,z') - h_b\right]\mathrm{d}z' \tag{30}$$

where h_u is the moist static energy in the updraft with fractional entrainment rate λ and h^* is the saturation moist static energy. For a given plume or cloud type, organized detrainment is assumed to take place only at the cloud top. Since a spectrum of plumes is considered, organized detrainment for the cloud population can occur at all levels, unlike that in the Tiedtke scheme, where it can only occur at the topmost level:

$$D_u(z) = -m_u(\lambda_D(z),z)\frac{\mathrm{d}\lambda_D(z)}{\rho\mathrm{d}z} \tag{31}$$

With this, the total updraft mass entrainment E_u can be obtained from the mass continuity equation (18). Once the vertical distribution of cloud mass flux is known, the other cloud properties can be obtained from Eqs. (19) – (25).

Note that the fractional turbulent entrainment rate for a given cloud type is assumed to be constant with height in steady-state cloud models. However, recent studies have found that convective entrainment varies significantly with height[27-29]. This subject has always been an area of active research due to its importance in determining the timing of convection from diurnal cycle to Madden-Julian Oscillation.

The downdraft model is similar to an inverted updraft. The downdraft mass flux at the downdraft initial level is often related to the updraft mass flux at the cloud base with a proportionality constant based on Johnson[30]. Furthermore, detrainment of downdraft mass is often ignored until the subcloud layer, and the entrainment rate is either specified or related to the updraft entrainment. Details can be found in [9].

2.1.2 Episodic mixing model

The entraining plume model assumes that subcloud-layer air mixes thoroughly and continually with the environmental air as it rises in updrafts. On the other hand, Raymond and Blyth[31] introduced a stochastic mixing model, which assumes that an individual subcloud-layer air parcel undergoes only one mixing event on its way to the neutral buoyancy level where it detrains. Based on this episodic mixing concept, Emanuel[7] used a stochastic mixing model to represent convective updrafts. In this model, each cloud of scale O (1km) consists of sub-cloud scale O (100m) updrafts. An updraft rising from the cloud base to a level has an equal probability of mixing with air from all levels during its ascent. The mixed air then undergoes a further ascent or a descent to its neutral buoyancy level for detrainment, depending on the buoyancy of the mixture. In this buoyancy-sorting approach, cloud mass flux profile is determined by the vertical gradient of buoyancy[32]. Fig. 2 shows the flow chart of the mixing model. The detailed mathematical formulation of the model is complicated and is not presented here. Interested readers are referred to Emanuel[7] and Emanuel and Zivkovic-Rothman[32] for details.

2.2 Closure conditions

The system of equations for convective parameterization is not closed without specifying the cloud base mass flux. This is achieved through closure assumptions, which empirically relate cloud base mass flux to observable variables or quantities that can be derived from observed fields.

2.2.1 Moisture convergence closure

Tiedtke[5] related low-level moisture convergence to the cloud base mass flux. It was assumed that moisture supply in the subcloud layer through large-scale horizontal convergence and surface turbulent flux is depleted by convective transport through the cloud base:

$$\left[M_u(q_u-\overline{q})+M_d(q_d-\overline{q})\right]_{z=z_b}=-\int_0^{z_b}\left[\overline{\boldsymbol{v}}\cdot\nabla\overline{q}+\overline{w}\frac{\partial\overline{q}}{\partial z}\right]\overline{\rho}\mathrm{d}z+(\overline{\rho}\overline{w'q'})_{tur} \quad (32)$$

where the last term on the right hand side represents surface turbulent moisture flux.

2.2.2 CAPE closure

Zhang et al.[9] used CAPE (convective available potential energy) as closure. Since the large-scale temperature and moisture changes in both the cloud layer and the subcloud layer due to convective activity are linearly related to the cloud base mass flux, *CAPE* change due to convection can be written as

$$\left(\frac{\partial CAPE}{\partial t}\right)_{cu}=-M_bK \quad (33)$$

where K is the *CAPE* consumption rate by convection per unit cloud base updraft mass flux, and is determined by the large-scale thermodynamic profiles and the cloud model. In practice, it is obtained by computing *CAPE* reduction in models for unit cloud base mass flux. The closure condition is that the *CAPE* is removed at an exponential rate by convection with a characteristic adjustment time scale τ. Thus

$$M_b=\frac{CAPE}{\tau K} \quad (34)$$

where τ is typically a few hours. This type of closure has been used in the NCAR CAM[9], the ECMWF Integrated Forecast System[33] and the Hadley Centre climate model HadAM3[34]. Some variants of CAPE-based closure are also used in the Emanuel scheme[7] and Kain-Fritsch scheme [35].

2.2.3 Quasi-equilibrium closure

The Arakawa-Schubert (A-S) parameterization scheme is closed through a quasi-equilibrium assumption, which states that the stabilization of the atmosphere by convection is in quasi-equilibrium with the destabilization by large-scale processes. Arakawa-Schubert introduced the "cloud work function", which is similar to *CAPE* but with consideration of entrainment. Since the Arakawa-Schubert scheme uses a spectral cloud model, the quasi-equilibrium closure is applied to each subensemble of clouds. The convective stabilization is related to the grid-resolvable destabilization for each cloud type:

$$\frac{\mathrm{d}A_c(\lambda)}{\mathrm{d}t}=-\frac{\mathrm{d}A_{ls}(\lambda)}{\mathrm{d}t}\approx-\frac{A_{ls}^{t+\Delta t}(\lambda)-A^{t-\Delta t}(\lambda)}{2\Delta t} \quad (35)$$

where $\mathrm{d}A_c(\lambda)/\mathrm{d}t$ and $\mathrm{d}A_{ls}(\lambda)/\mathrm{d}t$ are the time rate of change of cloud work function due to convective and the large-scale processes, respectively. $A_{ls}^{t+\Delta t}(\lambda)$ is the cloud work function at time t after the large-scale forcing is applied, $A^{t-\Delta t}$ is the observed cloud work function at $t-\Delta t$ (after convection), Δt is the time interval of the observations.

In all implementations of the A-S scheme in GCMs, climatological values are used for the observed cloud work functions following Lord[26]. Thus, Eq. (35) can be written as:

$$\frac{\mathrm{d}A_c(\lambda)}{\mathrm{d}t} \approx -\frac{A_{ls}^{t+\Delta t}(\lambda)-A_0(\lambda)}{2\Delta t} \tag{36}$$

Similar to the *CAPE* closure, the change in cloud work function by convection is proportional to the cloud base mass flux:

$$\frac{\mathrm{d}A_c(\lambda)}{\mathrm{d}t} = -K(\lambda)m_b(\lambda) \tag{37}$$

where $K(\lambda)$ can be computed from the large-scale conditions and the spectral cloud model. Thus, the closure equation becomes:

$$m_b(\lambda) = \frac{1}{K(\lambda)}\frac{A_{ls}^{t+\Delta t}(\lambda)-A_0(\lambda)}{2\Delta t} \tag{38}$$

This is similar to the *CAPE* closure, except using cloud work function and it is applied to every cloud type.

2.2.4 Free tropospheric quasi-equilibrium closure

Zhang[36-37] revisited the A-S quasi-equilibrium using data in both midlatitude land convection and tropical oceanic convection regimes using observational data, and found that the A-S does not hold well in either regime. He introduced a free tropospheric quasi-equilibrium as a refinement to the A-S quasi-equilibrium. Since *CAPE* is the vertical integral of the difference of a parcel's virtual temperature and that of its environment, *CAPE* (denoted by A hereafter) change with time can be a result of either the parcel's virtual temperature change or its environmental virtual temperature change, that is,

$$\frac{\mathrm{d}A}{\mathrm{d}t} = \frac{\mathrm{d}A_p}{\mathrm{d}t} + \frac{\mathrm{d}A_e}{\mathrm{d}t} \tag{39}$$

where subscript p is for parcel and e for environment. Zhang[36] found that *CAPE* change is largely controlled by the parcel's virtual temperature change. In other words, $\frac{\mathrm{d}A_e}{\mathrm{d}t} \approx 0$. Same as for the cloud work function, the environmental contribution to *CAPE* change is due to two types of processes: convective processes and large-scale processes:

$$\frac{\mathrm{d}A_e}{\mathrm{d}t} = \left(\frac{\mathrm{d}A_e}{\mathrm{d}t}\right)_c + \left(\frac{\mathrm{d}A_e}{\mathrm{d}t}\right)_{ls} \approx 0 \tag{40}$$

Eq. (40) forms the basis of the free tropospheric quasi-equilibrium. It states that convective contribution to the free tropospheric *CAPE* change balances the large-scale contribution. From this assumption, convective cloud base mass flux can be estimated in a similar way to that of the A-S scheme [Eqs. (35)–(38)].

2.2.5 Prognostic closure

The above closure conditions are all diagnostic. A serious drawback with diagnostic closures is that they cannot account for the history or memory of convection. Pan et al. [38] explored a prognostic closure under the framework of the Arakawa-Schubert convection parameterization. Instead of assuming a quasi-equilibrium between convective and large-scale processes, they predict column-integrated subgrid scale eddy kinetic energy, which is presumably associated with convective circulation. The equation is given by

$$\frac{\partial K}{\partial t} = AM_b - \frac{K}{\tau_D} \tag{41}$$

where $K = \frac{1}{2}\int_{Z_s}^{Z_t} \rho(\overline{u'^2}+\overline{v'^2}+\overline{w'^2})$ is the total eddy kinetic energy integrated from the surface to the cloud top, A is the cloud work function, M_b is the cloud base mass flux, and τ_D is the dissipation timescale for eddy kinetic energy, a tuning parameter. Pan et al. [38] further related K to M_b through the following assumption

$$K = \alpha M_b^2 \tag{42}$$

where α is another tuning parameter. Eqs. (41) and (42) form the prognostic closure, in which the cloud base mass flux is predicted. Despite its attractiveness of accounting for convection history in a prognostic closure, there has not been much further progress along this line of research until recently. Chikira et al. [39] modified the A-S scheme by incorporating the prognostic closure together with a modified entrainment formulation. Chikira[40] showed that the modified A-S scheme realistically simulated many climatological features of the global climate.

2.2.6 Examples

As an example to demonstrate the accuracy of different closures, Fig. 3 shows the scatter plots of the diagnosed total *CAPE* change due to convection using Eq. (35) (Fig. 3a) and partial *CAPE* change due to convection using Eq. (40) (Fig. 3b) using data from the US Southern Great Plains during the field campaign period of 19 June to 18 July 1997 by the US Department of Energy Atmospheric Radiation Measurement (ARM) program.

The line with a slope of –1 corresponds to the strict A-S quasi-equilibrium at the top and the free tropospheric quasi-equilibrium at the bottom, respectively. Although the diagnosed total *CAPE* changes due to convection based on the A-S closure are in general correlated with the large-scale generation of the total *CAPE*, there is a significant degree of scatter. On the other hand, the diagnosed partial *CAPE* change due to convection using the free tropospheric quasi-equilibrium closure is in much better agreement with that from large-scale forcing.

The free tropospheric quasi-equilibrium closure has been tested in the U.S. National Center for Atmospheric Research Community Atmosphere Model 3 (NCAR CAM3). A number of significant improvements on the simulation of tropical climate have been achieved, including the simulation of Madden-Julian Oscillation and the Intertropical Convergence Zone[41-43]. Fig. 4 demonstrates the improvement in MJO simulation by showing the characteristics of the simulated MJOs through longitude-phase hovmöller plots of composite 850 hPa zonal wind, precipitation and outgoing longwave radiation (OLR) averaged over 10ºS–10ºN for the observations, the CAM3 run with the quasi-equilibrium closure in convection scheme, and CAM3 control run, respectively. The results are based on 10-yr long simulations by Zhang et al. [41-43]. Phases 1, 5 and 9 correspond to the beginning, mature phase and the end of the MJO cycle, respectively. The observations show clear eastward propagation in 850 hPa zonal wind, precipitation and OLR. In the new CAM3 simulation, the eastward propagation of the MJO signals in all three fields is well simulated. The magnitude of the MJO signals is also comparable to the observations. On the other hand, in the CAM3 control simulation, the MJO signal in zonal wind, precipitation and OLR are very weak everywhere, although there is a hint of eastward propagation.

3. Parameterization of convective momentum transport

Convection transports not only heat and moisture, but also momentum. In the early 1970's, budget analysis found that the Earth's angular momentum could not be balanced without considering momentum transport by convection[44]. Later, Schneider and Lindzen[45] proposed a parameterization scheme for convective momentum transport (CMT). Similar to thermodynamic parameterization, the large-scale effect of convection on momentum can be written as:

$$\begin{aligned} \boldsymbol{X} &\equiv \frac{\partial \overline{\boldsymbol{v}}}{\partial t}+\overline{\boldsymbol{v}}\cdot\nabla\overline{\boldsymbol{v}}+\overline{\omega}\frac{\partial \overline{\boldsymbol{v}}}{\partial p}+\nabla\overline{\phi}+f\boldsymbol{k}\times\overline{\boldsymbol{v}}=-\nabla\cdot\overline{\boldsymbol{v}'\boldsymbol{v}'}-\frac{\partial\overline{\boldsymbol{v}'\omega'}}{\partial p} \\ &\simeq g\frac{\partial M_c(\boldsymbol{v}_c-\overline{\boldsymbol{v}})}{\partial p}\simeq-\frac{\partial M_c(\boldsymbol{v}_c-\overline{\boldsymbol{v}})}{\rho\partial z} \end{aligned} \tag{43}$$

where M_c is cloud mass flux and $\boldsymbol{v}_c$ is the horizontal momentum of in-cloud air. The difficulty lies in determining the cloud mean momentum. Unlike the thermodynamic variables such as moist static energy, even for undiluted updrafts, momentum is not conserved due to the action of convection-induced pressure gradient force across the clouds.

The convection-induced pressure gradient force contributes to the apparent momentum source $\boldsymbol{X}$ through its effect on the cloud-mean momentum $\boldsymbol{v}_c$. For steady-state clouds, momentum equation in convective clouds is approximated by:

$$D\boldsymbol{v}_c-E\overline{\boldsymbol{v}}+\frac{\partial(M_c\boldsymbol{v}_c)}{\rho\partial z}=-\frac{1}{\rho}\sigma_c(\nabla p)_c \tag{44}$$

where E and D are the mass entrainment and detrainment at the cloud boundaries and satisfy the mass continuity equation

$$\frac{\partial M_c}{\rho\partial z}=E-D$$

Substituting these into momentum source equation gives:

$$\boldsymbol{X}=M_c\frac{\partial\overline{\boldsymbol{v}}}{\rho\partial z}+D(\boldsymbol{v}_c-\overline{\boldsymbol{v}})+\frac{1}{\rho}\sigma_c(\nabla p)_c \tag{45}$$

The first term is the product of the updraft mass flux and the vertical wind shear, and is often interpreted as the vertical advection by the compensating subsidence in the cloud environment; the second represents the horizontal momentum detrainment from convective updrafts into their environment; the last term is the pressure gradient across the clouds. Schneider et al. [45] ignored the convective pressure effect.

Field observations of convective storms during the 1980's found that convection can produce large pressure perturbations in and around the storm, which can modulate the horizontal momentum inside the clouds[46-47]. To incorporate such effects of the perturbation pressure field, Zhang et al. [10-11] started with the 3-D momentum equation:

$$\rho\frac{\partial\boldsymbol{v}_3}{\partial t}+\rho\boldsymbol{v}_3\cdot\nabla_3\boldsymbol{v}_3+2\rho\boldsymbol{\Omega}\times\boldsymbol{v}_3=-\nabla p+\boldsymbol{k}\rho B \tag{46}$$

where $\boldsymbol{v}_3=(u,v,w)$ is the 3-D wind vector, $\boldsymbol{\Omega}$ is the vector form of the Coriolis parameter, and B is buoyancy of the cloud air. Note that $\boldsymbol{v}_3\cdot\nabla_3\boldsymbol{v}_3+2\boldsymbol{\Omega}\times\boldsymbol{v}_3=\nabla_3(\frac{1}{2}\boldsymbol{v}_3\cdot\boldsymbol{v}_3)+\boldsymbol{\eta}\times\boldsymbol{v}_3$, where $\boldsymbol{\eta}=\nabla_3\times\boldsymbol{v}_3+2\boldsymbol{\Omega}$ is 3-D absolute vorticity. Taking the

3-D divergence operation on the 3-D momentum equation and making use of mass continuity equation, one gets:

$$\begin{aligned}\nabla_3^2 p &= -\nabla_3\left(\frac{\rho}{2}\nabla_3\boldsymbol{v}_3\cdot\boldsymbol{v}_3\right)-\nabla_3\cdot(\rho\boldsymbol{\eta}\times\boldsymbol{v}_3)+\nabla_3\cdot(\rho\boldsymbol{k}B)\\ &= -\nabla_3^2\left(\frac{\rho}{2}\boldsymbol{v}_3\cdot\boldsymbol{v}_3\right)+\nabla_3\cdot\left(\frac{1}{2}\boldsymbol{v}_3\cdot\boldsymbol{v}_3\nabla_3\rho\right)+\rho\eta^2+\boldsymbol{v}_3\cdot(\nabla_3\times\rho\boldsymbol{\eta})+\nabla_3\cdot(\rho\boldsymbol{k}B)\end{aligned} \quad (47)$$

The buoyancy force is important for creating vertical pressure gradient. Its effect on horizontal pressure gradient across convective clouds depends on the cloud tilting[46]. Since we do not have enough knowledge about it, it is ignored in CMT parameterization. Expanding Eq. (47) gives:

$$\nabla_3^2 p = -2\rho\left[\frac{\partial w}{\partial x}\frac{\partial u}{\partial z}+\frac{\partial w}{\partial y}\frac{\partial v}{\partial z}+\frac{\partial v}{\partial x}\frac{\partial u}{\partial y}\right]-\rho\left[(\frac{\partial u}{\partial x})^2+(\frac{\partial v}{\partial y})^2+(\frac{\partial w}{\partial z})^2\right]+w^2\rho\frac{\partial}{\partial z}\left(\frac{1}{\rho}\frac{\partial\rho}{\partial z}\right) \quad (48a)$$

Zhang et al.[10,11] solved Eq. (48a) using Fourier and Bessel expansions together with appropriate upper and lower boundary conditions to obtain the mean pressure gradient force across clouds. Zhang et al.[48] assessed the effect of CMT on climate simulation and found large impacts on the mean climate. Later work found that CMT can also have impacts on the simulations of El Nino and Madden-Julian Oscillation[49-50].

Simplified forms of the representation of perturbation pressure gradient force have been investigated after Zhang and Cho's work. For a harmonic waveform horizontal variation in convective vertical velocity and perturbation pressure, this can be achieved. The forcing on the rhs of Eq. (48) can be divided into linear and nonlinear components.

$$\begin{aligned}\nabla_3^2 p = &-2\rho\frac{\partial w}{\partial x}\frac{\partial\overline{u}}{\partial z}-2\rho\frac{\partial w}{\partial y}\frac{\partial\overline{v}}{\partial z}-2\rho\frac{\partial w}{\partial x}\frac{\partial u'}{\partial z}-2\rho\frac{\partial w}{\partial y}\frac{\partial v'}{\partial z}\\ &-\rho\left[(\frac{\partial u}{\partial x})^2+(\frac{\partial v}{\partial y})^2+(\frac{\partial w}{\partial z})^2\right]+w^2\rho\frac{\partial}{\partial z}\left(\frac{1}{\rho}\frac{\partial\rho}{\partial z}\right)\end{aligned} \quad (48b)$$

The first two terms on the rhs are the linear forcing, proportional to the vertical shear of the mean wind. The remainder represents nonlinear forcing, of which the first term is related to the perturbation wind shear, the terms inside the square brackets are related to the divergent flow and the third term is related to the atmospheric stratification. Consider the linear forcing only:

$$\nabla_3^2 p \approx -2\rho\frac{\partial w}{\partial x}\frac{\partial\overline{u}}{\partial z}-2\rho\frac{\partial w}{\partial y}\frac{\partial\overline{v}}{\partial z}$$

Assume w is of a sine form:

$$w = w_0\cos kx\cos ly\sin mz \text{ for } -\frac{\pi}{2}<kx,ly<\frac{\pi}{2}$$

where, k, l, and m are wavenumbers in the x-, y- and z-direction, respectively. Then

$$\begin{aligned}p &= \frac{2\rho}{k^2+l^2+m^2}\left(\frac{\partial\overline{u}}{\partial z}k\sin kx\cos ly+\frac{\partial\overline{v}}{\partial z}l\cos kx\sin ly\right)w_0\sin mz\\ \frac{1}{\rho}\frac{\partial p}{\partial x} &= \frac{2w_0}{k^2+l^2+m^2}\left(\frac{\partial\overline{u}}{\partial z}k^2\cos kx\cos ly-\frac{\partial\overline{v}}{\partial z}kl\sin kx\sin ly\right)\sin mz\\ \frac{1}{\rho}\frac{\partial p}{\partial y} &= \frac{2w_0}{k^2+l^2+m^2}\left(-\frac{\partial\overline{u}}{\partial z}kl\sin kx\sin ly+\frac{\partial\overline{v}}{\partial z}l^2\cos kx\cos ly\right)\sin mz\end{aligned}$$

Averaging over the cloud area gives:

$$\frac{\sigma_c}{\rho}(\frac{\partial p}{\partial x})_c = -\frac{2k^2}{k^2+l^2+m^2}\frac{\partial\overline{u}}{\partial z}\sigma_c w_c = -\gamma_x M_c\frac{\partial\overline{u}}{\rho\partial z} \quad (49a)$$

$$\frac{\sigma_c}{\rho}(\frac{\partial p}{\partial y})_c = -\frac{2l^2}{k^2+l^2+m^2}\frac{\partial\overline{v}}{\partial z}\sigma_c w_c = -\gamma_y M_c\frac{\partial\overline{v}}{\rho\partial z} \quad (49b)$$

γ_x and γ_y are coefficients depending on the horizontal and vertical scales of the convective cloud. Thus, convection-induced pressure gradient depends on the horizontal as well as vertical scales of convective updrafts, in addition to mass flux and wind shear. For a convective updraft with about equal sizes in both horizontal and vertical directions, i.e. $k=l=m$, $\gamma_x=\gamma_y=0.67$.

Wu et al.[12] first used this approach. Later, Gregory et al.[13] used a cloud-resolving model simulation to estimate this parameter, and found that $\gamma=0.7$ is a good approximation. Zhang et al.[51] also evaluated the role

of convective pressure gradient force in CMT using a cloud-resolving model simulation of a TOGA COARE convection event, and found that γ=0.55 gives a better agreement. Substituting Eq. (49) into Eq. (45) gives:

$$\boldsymbol{X} = (1-\gamma)M_c \frac{\partial \overline{\boldsymbol{v}}}{\rho \partial z} + \delta(\boldsymbol{v}_c - \overline{\boldsymbol{v}}) \qquad (50)$$

Fig. 5 shows the x-component of pressure gradient force averaged over convective updraft and the convective effect on CMT, also called apparent momentum source, from Zhang et al.[51]. The cloud-mean pressure gradient force obtained by solving the full perturbation pressure equation as in Zhang et al.[10-11] is in excellent agreement with the model simulation. A least-squared fit using eq. (49) with γ=0.55 also produces a close agreement. The parameterized apparent momentum source captures the major features of the simulated CMT although the magnitude is somewhat larger.

4. Discussions and concluding remarks

Many of the convective parameterization schemes reviewed in this paper have been used widely in global atmospheric prediction and climate models. The Tiedtke scheme is used in the European Centre for Medium-Range Weather Forecasts (ECMWF) operational model[52]. The Emanuel scheme is used in the US Navy Operational Global Atmospheric Prediction System[53]. The Zhang-McFarlane scheme is used in the NCAR GCM[41-42]. The Arakawa and Schubert scheme is used in US National Centers for Environmental Prediction (NCEP)[54]. While the performance of a convective parameterization scheme depends on many factors including the parent model, some common weaknesses of the existing convection schemes are well known. Among them are double Intertropical Convergence Zones, weak MJO, wrong diurnal cycle of convection and too frequent weak precipitation and lack of high intensity precipitation. These model deficiencies point to the need of further improvements in convective parameterization. There have been some interesting progress recently in this regard.

As mentioned earlier, treatment of microphysical processes inside convective updrafts has received considerable interests in recent years. This is because detrained cloud hydrometeor is an important source of cloud water and ice for large-scale cloud development. In addition, reducing uncertainties in aerosol-convection interaction and aerosol indirect effect on clouds requires more accurate parameterization of convective microphysics. The recent work of [14-17] opened the door to a new line of research in this direction.

There has also been significant advancement in "superparameterization" or multi-scale modeling framework (MMF), which replaces the conventional convection parameterization by embedding a cloud-system-resolving model in a GCM[55-57]. While this approach generally produces better simulations than convectional parameterization schemes[58], it is computationally expensive. For climate projection research, which requires ensemble simulations of hundreds or even thousands of years, it is not feasible at least in the next decade. However, while it does not replace convective parameterization in any foreseeable future, it is an excellent tool for evaluating and improving conventional convective parameterization.

One of the outstanding issues facing convection parameterization today is its resolution dependence. Numerical weather prediction models will likely approach 5 km or higher and GCMs will approach 10 km resolutions in the next 5 to 10 years. At these resolutions, the separation between grid-scale motion and deep convection is no longer clear. To what extent are current convection schemes still usable? As mentioned before [Eqs. (14)–(15)], all convection schemes assume that convective cloud fraction within a model grid box is much smaller than 1. While this assumption is in general valid for model grid spacing of 100 km or larger, it will break down when model grid spacing is reduced to 10 km or smaller. At such high resolutions, convective cloud fraction can easily reach 0.5 or larger, and convection schemes need to be reformulated. Arakawa et al.[59-60] have explored the possibility of reformulating convective parameterization when cloud fraction is non-negligible. They argue that by introducing an additional equation for cloud fraction, existing parameterization schemes can be modified for use in high-resolution numerical models. This type of work is still in its infancy, and much more needs to be done to provide a sound foundation for convection parameterization in high-resolution numerical models.

Another issue is determining the vertical velocity in convective clouds, particularly in updrafts. Updraft vertical velocities are important for convective microphysical processes including droplet activation and ice nucleation by aerosols. They can also be used to determine convective cloud fraction, given updraft cloud mass flux. In addition, recent work on entrainment

estimation used in convection parameterization requires knowledge of updraft vertical velocity.

Finally, sub-grid scale variability and trigger conditions for convection initiation are important issues for convection parameterization. Currently, convection schemes use grid-mean properties to diagnose convective activity. In reality, convective plumes are strongly tied to local, sub-grid scale features such as cold pool currents/gust fronts and warm thermals. As for trigger conditions for convection onset, they determine the timing of convection. The wrong diurnal cycle of simulated convection in GCMs may well be related to inadequate convection trigger functions. Yet, all trigger functions in existing convection schemes are *ad hoc*, without systematic evaluation with observations or cloud model simulations. Anecdotal research[52,54] indicates that trigger functions have an important impact on climate simulation. Thus, a more systematic evaluation of trigger functions is needed.

This paper aims to provide a comprehensive review of convective parameterization schemes used in climate and numerical weather prediction models, with emphasis on mass flux type of schemes. A 1-dimentional steady-state cloud model is presented to demonstrate its use for determining cloud properties needed in convection parameterization. A stochastic mixing model is also discussed. Several closure conditions are described to illustrate our current understanding of the problem. One section is devoted to describing the parameterization of convective momentum transport. The difficulty of parameterizing CMT lies in estimating the effect of convection-induced perturbation pressure gradient force. Some outstanding issues facing convection parameterization developers and the general climate modeling /numerical weather prediction communities are briefly outlined.

参考文献

[1] Manabe S, Smagorinsky J, Strickler R F. Simulated climatology of a general circulation model with a hydrological cycle. Mon Wea Rev, 1965, 93: 769-798.

[2] Betts A K. A new convective adjustment scheme. I. Observational and theoretical basis. Quart J Roy Meteor Soc, 1986, 112: 677-691.

[3] Kuo H-L. On the formation and intensification of tropical cyclones through latent heat release by cumulus convection. J Atmos Sci, 1965, 22: 40-63.

[4] Kuo H L. Further studies of the parameterization of the influence of cumulus convection on large-scale flow. J Atmos Sci, 1974, 31: 1232-1240.

[5] Tiedtke M. A comprehensive mass flux scheme for cumulus parameterization in large-scale models. Mon Wea Rev, 1989, 117: 1779-1800.

[6] Arakawa A, Schubert W H. Interaction of a cumulus cloud ensemble with the large-scale environment. Part I. J Atmos Sci, 1974, 31: 674-701.

[7] Emanuel K A. A scheme for representing cumulus convection in large-scale models. J Atmos Sci, 1991, 48: 2313-2335.

[8] Donner L J. A cumulus parameterization including mass fluxes, vertical momentum dynamics, and mesoscale effects. J Atmos Sci, 1993, 50: 889-906.

[9] Zhang G J, McFarlane N A. Sensitivity of climate simulations to the parameterization of cumulus convection in the Canadian Climate Centre general circulation model. Atmosphere-Ocean, 1995, 33: 407-446.

[10] Zhang G J, Cho H R. Parameterization of the vertical transport of momentum by cumulus clouds. Part I: Theory. J Atmos Sci, 1991, 48: 1483-1492.

[11] Zhang G J, Cho H R. Parameterization of the vertical transport of momentum by cumulus clouds. Part II: Application. J Atmos Sci, 1991, 48: 2448-2457.

[12] Wu X, Yanai M. Effects of vertical wind shear on the cumulus transport of momentum: Observations and parameterization. J Atmos Sci, 1994, 51: 1640-1660.

[13] Gregory D, Kershaw R, Innes P M. Parameterization of momentum transport by convection. II: Tests in single column and general circulation models. Quart J Roy Meteor Soc, 1997, 123: 1153-1183.

[14] Zhang J H, Lohmann U, Stier P. A microphysical parameterization for convective clouds in the ECHAM5 climate model: Single-column model results evaluated at the Oklahoma Atmospheric Radiation Measurement Program site. J Geophys Res, 2005, 110, doi:10.1029/2004JD005128, D15S07.

[15] Lohmann U. Global anthropogenicaerosol effects on convective clouds in ECHAM5-HAM, Atmos Chem Phys, 2008, 8: 2115-2131.

[16] Song X, Zhang G J. Microphysics parameterization for convective clouds in a global climate model: Description and single-column model tests. J Geophys Res, 2011, 116: D02201, doi:10.1029/2010JD014833.

[17] Song X, Zhang G J, Li J-L. Evaluation of microphysics parameterization for convective clouds in the NCAR Community Atmosphere Model CAM5. J Climate, 2012, 25: 8568-8590, doi: 10.1175/JCLI-D-11-00563.1.

[18] IPCC. Climate Change 2007//Solomon S, et al. The Scientific Basis. Contribution of Working Group I to the Fourth Assessment Report of the Intergovernmental Panel on Climate Change. New York: Cambridge Univ.

[19] Rosenfeld D, Lohmann U, Raga G B, et al. Flood or drought: How do aerosols affect precipitation? Science, 2008, 321: 1309-1313.

[20] Li Z, Niu F, Fan J, et al. Long-term impacts of aerosols on the vertical development of clouds and precipitation. Nature Geoscience, 2011, 4: 888-894, doi:10.1038/ngeo1313.

[21] Malkus J S, Riehl H. On the dynamics and energy transformations in steady state hurricanes. Tellus, 1960, 12: 1-20.

[22] Arakawa A. Parameterization of cumulus convection. Proc WMO/IUGG Symp. Numerical Weather Prediction. Japan Meteor Agency, 1969, IV(8): 1-6.

[23] Ooyama K. A theory on parameterization of cumulus convection. J Meteor Soc Japan, 1971, 49(S): 744-756.

[24] Krishnamurti T N, Ramanathan Y, Pan H-L, et al. Cumulus parameterization and rainfall rates I. Mon Wea Rev, 1980, 108: 465-472.

[25] Yanai M, Esbensen S, Chu J H. Determination of bulk properties of tropical cloud clusters from large-scale heat and moisture budgets. J Atmos Sci, 1973, 30: 611-627.

[26] Lord S J. Interaction of a cumulus cloud ensemble with large-scale environment. Part III: Semi-prognostic test of the Arakawa-Schubert cumulus parameterization. J Atmos Sci, 1982, 39: 88-103.

[27] Neggers R A J, Siebesma A P, Jonker H J J. A multiparcel model for shallow cumulus convection. J Atmos Sci, 2002, 59: 1655-1668.

[28] Del Genio A D, Wu J. The role of entrainment in the diurnal

cycle of continental convection, J Clim, 2010, 23: 2722-2738, doi: 10.1175/2009JCLI3340.1.
[29] Romps D. A direct measure of entrainment. J Atmos Sci, 2010, 67: 1908-1927.
[30] Johnson R H. Cumulus transports in a tropical wave composite for phase III of GATE. J Atmos Sci, 1978, 35: 484-494.
[31] Raymond D J, Blyth A M. A stochastic model for nonprecipitating cumulus clouds. J Atmos Sci, 1986, 43: 2708-2718.
[32] Emanuel K A, Zivkovic-Rothman M. Development and evaluation of a convection scheme for use in climate models. J Atmos Sci, 1999, 56: 1766-1782
[33] Gregory D, Morcrette J J, Jacob C et al. Revision of convection, radiation and cloud schemes in the ECMWF Integrated Forecasting System. Quart J Roy Meteor Soc, 2000, 126: 1685-1710.
[34] Pope V D, Gallani M L, Rowntree P R, et al. The impact of new physical parameterizations in the Hadley Centre climate model: HadAM3. Climate Dyn, 2000, 16: 123-146.
[35] Kain J S, Fritsch J M. A one-dimensional entraining/detraining plume model and its application in convective parameterization. J Atmos Sci, 1990, 47: 2784-2802.
[36] Zhang G J. Convective quasi-equilibrium in midlatitude continental environment and its effect on convective parameterization. J Geophys Res, 2002, 107: doi: 10.1029/2001JD001005.
[37] Zhang G J. Convective quasi-equilibrium in the Tropical western Pacific: Comparison with midlatitude continental environment. J Geophys Res, 2003, 108: D19, 4592, doi:10.1029/2003JD003520.
[38] Pan V, Randall D A. A cumulus parameterization with a prognostic closure. Q J R Meteorol Soc, 1998, 124: 949-981.
[39] Chikira M, Sugiyama M. A cumulus parameterization with state-dependent entrainment rate. Part I: Description and sensitivity to temperature and humidity profiles. J Atmos Sci, 2010, 67: 2171-2193, doi:10.1175/2010JAS3316.1.
[40] Chikira M. A cumulus parameterization with state-dependent entrainment rate. Part II: Impact on climatology in a general circulation model. J Atmos Sci, 2010, 67: 2194-2211, doi:10.1175/2010JAS3317.1.
[41] Zhang G J, Mu M. Simulation of the Madden-Julian oscillation in the NCAR CCM3 using a revised Zhang-McFarlane convection parameterization scheme. J Climate, 2005, 18: 4049-4067.
[42] Zhang G J, Mu M. Effects of modifications to the Zhang-McFarlane convection parameterization on the simulation of the tropical precipitation in the National Center for Atmospheric Research Community Climate Model, version 3. J Geophys Res, 2005, 110 (D09109), doi:10.1029/2004JD005617.
[43] Zhang G J, Wang H. Toward mitigating the double ITCZ problem in NCAR CCSM3. Geophys Res Let, 2006, 33 (L06709), doi:10.1029/2005GL025229.
[44] Austin P M, Houze Jr. R A. A technique for computing vertical transports by precipitating cumuli. J Atmos Sci, 1973, 30: 1100-1111.
[45] Schneider E K, Lindzen R S. A discussion of the parameterization of momentum exchange by cumulus convection. J Geophys Res, 1976, 81: 3158-3161.
[46] LeMone M A. Momentum transport by a line of cumulonimbus. J Atmos Sci, 1983, 40: 1815-1834.
[47] LeMone M A, Barnes G M, Kankhauser J C, et al. Perturbation pressure fields measured by aircraft around the cloud base updraft of deep convective clouds. Mon Wea Rev, 1988, 116: 313-327.
[48] Zhang G J, McFarlane N A. Role of convective-scale momentum transport in climate simulation. J Geophy Res, 1995, 100: 1417-1426.
[49] GFDL Model Development Team. The GFDL new global atmosphere and land model AM2/LM2: Evaluation with prescribed SST simulations. J Climate, 2004, 17: 4641-4673.
[50] Deng L, Wu X. Effects of Convective Processes on GCM Simulations of the Madden–Julian Oscillation. J Climate, 2010, 23: 352–377, doi: 10.1175/2009JCLI3114.1
[51] Zhang G J, Wu X. Convective momentum transport and perturbation pressure field from a cloud-resolving model simulation. J Atmos Sci, 2003, 60: 1120-1139.
[52] Jakob C, Siebesma A P. A new subcloud model for mass-flux convective schemes—influence on triggering, updraught properties, and model climate. Mon Wea Rev, 2003, 131: 2765-2778.
[53] Peng M S, Ridout J A, Hogan T F. Recent modifications of the Emanuel convective scheme in the navy operational global atmospheric prediction system. Mon Wea Rev, 2004, 132, 1254-1268.
[54] Lee M-I, Schubert S D, Suarez M J, et al. An analysis of the warm-seasona diurnal cycle over the continental United States and North Mexico in general circulation models. J Climate, 2007, 20: 344-366, doi: 10.1175/JHM581.1.
[55] Grabowski W W. Coupling cloud processes with the large-scale dynamics using the cloud-resolving convection parameterization (CRCP). J Atmos Sci, 2001, 58: 978-997.
[56] Khairoutdinov M F, Randall D A. A cloud resolving model as a cloud parameterization in the NCAR Community System Model: Preliminary results. Geophys Res Lett, 2001, 28: 3617-3620.
[57] Tao W-K, Chern J, Atlas R, et al. A multiscale modeling system: Developments, applications, and critical issues. Bull Amer Meteor Soc, 2009, 90: 515-534.
[58] Stan C, Khairoutdinov M, DeMott C A, et al., An ocean-atmosphere climate simulation with an embedded cloud resolving model. Geophys Res Lett, 2009, 37: L01702, doi: 10.1029/2009GL040822.
[59] Arakawa A, Jung J H, Wu C M. Toward unification of the multiscale modeling of the atmosphere. Atmos Chem Phys, 2011, 11: 3731-3742.
[60] Arakawa A, Wu C-M. A unified representation of deep moist convection in numerical modeling of the atmosphere. Part I. J Atmos Sci, 2013, 70: 1977-1992.